

Aluminium Binding to Modified Amyloid- β Peptides: Implications for Alzheimer's Disease

Cosmin Stefan Mocanu, Monica Jureschi and Gabi Drochioiu *

Faculty of Chemistry, "Al. I. Cuza" University of Iasi, 11 Carol I, 70605 Iasi, Romania; cosmin.mocanu@chem.uaic.ro (C.S.M.); jureschi.monica@yahoo.com (M.J.)

* Correspondence: gabidr@uaic.ro; Tel.: +40-722-280328

Academic Editors: Luca D. D'Andrea and Lucia De Rosa

Received: 3 September 2020; Accepted: 2 October 2020; Published: 3 October 2020

Abstract: Aluminium (Al) is clearly neurotoxic and considerable evidence exists that Al may play a role in the aetiology or pathogenesis of Alzheimer's disease (AD). Nevertheless, the link between AD pathology and Al is still open to debate. Therefore, we investigated here the interaction of aluminium ions with two A β peptide fragments and their analogues. First, we synthesised by the Fmoc/tBu solid-phase peptide synthesis (SPPS) strategy using an automated peptide synthesiser two new peptides starting from the A β _(1–16) native peptide fragment. For this purpose, the three histidine residues (H⁶, H¹³, and H¹⁴) of the A β _(1–16) peptide were replaced by three alanine and three serine residues to form the modified peptides A β _(1–16)A₃^{6,13,14} and A β _(1–16)S₃^{6,13,14} (primary structures: H-¹DAEFRADSGYEVA¹⁶AQK¹⁶-NH₂ and H-¹DAEFRSDSGYEVSSQK¹⁶-NH₂). In addition, the A β _(9–16) peptide fragment (H-⁹GYEVHHQK¹⁶-NH₂) and its glycine analogues, namely A β _(9–16)G¹⁰₁ (H-⁹GGEVHHQK¹⁶-NH₂), A β _(9–16)G^{13,14}₂ (H-⁹GYEVGGQK¹⁶-NH₂), and A β _(9–16)G^{10,13,14}₃ (H-⁹GGEVGGQK¹⁶-NH₂), were manually synthesised in order to study Al binding to more specific amino acid residues. Both the peptides and the corresponding complexes with aluminium were comparatively investigated by mass spectrometry (MS), circular dichroism spectroscopy (CD), atomic force microscopy (AFM), scanning electron microscopy (SEM), and Fourier transform infrared spectroscopy (FT-IR). Al-peptide molecular ions and Al-fragment ions were unambiguously identified in the MS and MS/MS spectra. AFM images showed dramatic changes in the film morphology of peptides upon Al binding. Our findings from the investigation of N-terminal 1–16 and even 9–16 normal and modified sequences of A β peptides suggest that they have the capability to be involved in aluminium ion binding associated with AD.

Keywords: amyloid- β peptides; modified A β peptide fragments; aluminium ions; metal binding; mass spectrometry; circular dichroism spectroscopy; atomic force microscopy; FT-IR; Alzheimer's disease

1. Introduction

The prevalence of Alzheimer's disease (AD) continues to increase worldwide, becoming a great healthcare challenge of the twenty-first century [1]. AD is a progressive neurodegenerative disorder that gradually deprives the patient of cognitive function, being characterised by the presence of senile plaques and neurofibrillary tangles in the hippocampus and neocortex of the brain [2]. Intracranial amyloid aggregates, which are dependent on the proteolysis of the A β precursor protein (APP), are usually found in AD brains [3,4]. Such aggregates are made up of amyloid- β (A β) peptides, cholesterol, and metal ions and generate so-called neural plaques. The proteolytic A β peptides are normally degraded and removed, but they may accumulate in AD brains, mainly in presynaptic terminals of neurons to form insoluble plaques [5]. Peptide aggregates lead to the death of affected

hippocampal neurons [6]. A β plaques contribute to neuronal loss and ultimate failure of cognitive function [7]. The interaction of A β peptides with ions of copper, zinc, iron, aluminium, manganese, or mercury may contribute to neuronal damage [8–10]. Once A β begins to accumulate, it then promotes the build-up of Tau [11]. Hence, blocking the production and aggregation of A β peptides is of interest in AD therapy [12]. A β aggregation, a known contributor in AD pathogenesis, is triggered by several metal ions through occupational exposure and disrupted metal ion homeostasis [13]. Thus, amyloid- β aggregates are associated with AD and can be promoted by traces of metal ions such as aluminium, iron, zinc, copper, manganese, lead, cadmium, or mercury [14]. It is well known that these elements cause conformational changes of Alzheimer's amyloid- β peptides [15]. Although Al is a neurotoxic agent, the link of Al to the aetiology of various serious neurological disorders such as Alzheimer's disease (AD) remains controversial [16,17]. Nevertheless, Al has been included among the potential risk factors for the aetiology of AD [15,18]. Al may also accelerate the proteolytic processing of APP by suppression of the inhibitor domain in the Alzheimer's brain [19]. Moreover, Al induces the accumulation of A β peptides and tau protein in the brains of experimental animals [20]. As a result, the A β peptide may accumulate and initiate plaque formation. There is evidence that Al and A β are co-located in a senile plaque-like structure [21]. However, a natural phenolic antioxidant, curcumin, is capable of binding with Al ions, and the metal–curcumin complex can inhibit the transition from less structured oligomers to β -sheet-rich protofibrils [22].

Recently, multiple microsecond-long molecular dynamics simulations of complexes of amyloid- β peptides with aluminium ions have also been reported [23]. On the other hand, in order to highlight the importance of each amino acid residue from the A β region involved in the formation of complexes with amyloidogenic substances, peptides containing alanine single-site mutations within the A β binding sequence can be produced by solid-phase peptide synthesis, whereas the complex formation could be investigated for each mutant peptide by mass spectrometry (MS) [24]. Mass spectrometric investigation of non-covalent complex formation between amyloid- β peptides and various toxic substances tested for their impact in AD is an important step for clarifying their mechanism of action [25]. Experiments based on MS, infrared (IR), UV–vis and microscopic techniques revealed significant changes in the structure of peptides, including their aggregation and fibrillation, associated with metal binding [26–29]. We have recently been looking for evidence of such complexity using MS and other bioanalytical techniques [30–32].

Very little is also known about how pH and time-dependent metal ion binding to specific A β sequences influence the structure, aggregation, fibrillation, and plaque formation in vitro and in AD brains [33,34]. Therefore, we aimed in this study to address this knowledge gap and determine the relative contribution of aluminium binding of several A β analogue peptides. Towards this goal, we used a combination of MS, circular dichroism spectroscopy (CD), atomic force microscopy (AFM), SEM, FT-IR, and other techniques to establish the role played by the three histidine residues of the A β _(1–16) sequence in binding aluminium ions, if any. We followed the hypothesis that replacing the histidine residues in positions 6, 13, and 14 of A β _(1–16) peptide fragment sequence H-¹DAEFRHDSGYEVHHQK¹⁶-NH₂ with alanine [24] or serine may result in two new variants of A β _(1–16) peptide that may afford a different pattern of interaction with Al ions. Consequently, the modified peptides A β _(1–16)A_{36,13,14} (H-¹DAEFRADSGYEVA^{36,13,14}AQK¹⁶-NH₂) and A β _(1–16)S_{36,13,14} (H-¹DAEFRSDSGYEVSSQK¹⁶-NH₂) were synthesised by the Fmoc/*t*Bu solid-phase peptide synthesis (SPPS) strategy and purified by reverse phase-high performance liquid chromatography (RP-HPLC). Furthermore, because the amino acid residues Glu³, Asp⁷, and Glu¹¹ are suspected to bind Al [23], we decided to use in our experiments the smaller peptide A β _(9–16) and several analogues, which do not contain the first two amino acid residues in their sequences. Consequently, in the sequence of the A β _(9–16) peptide fragment (GYEVHHQK), we replaced either the histidine residues or the tyrosine one with glycine to form new molecules of more flexible peptides, namely A β _(9–16)G₁₁₀ (GGEVHHQK), A β _(9–16)G_{213,14} (GYEVGGQK), and A β _(9–16)G_{310,13,14} (GGEVGGQK). Finally, matrix-assisted laser desorption ionization time-of-flight (MALDI-ToF) mass spectrometry, including MS/MS study, and Fourier transform infrared (FT-IR) spectroscopy revealed an unexpected pattern of aluminium ion binding to both A β _(1–16) and A β _(9–16) peptides and its analogues.

2. Results

2.1. Peptide Synthesis

First, two modified peptides, analogues of the $A\beta_{(1-16)}$ peptide fragment, were synthesised by SPPS according to the Fmoc/*t*-Bu strategy on an automated peptide synthesiser. In the native $A\beta_{(1-16)}$ peptide, which was also synthesised under the same conditions, the three histidine residues were replaced with alanine ($A\beta_{(1-16)}A_{3^{6,13,14}}:H^{-1}DAEFRADSGYEVAQK^{16}-NH_2$) and serine ($A\beta_{(1-16)}S_{3^{6,13,14}}:H^{-1}DAEFRSDSGYEVSSQK^{16}-NH_2$), in order to produce two peptides lacking the imidazole ring but with similar flexibility to the native $A\beta_{(1-16)}$ peptide. The serine-rich peptide also contains more hydroxyl groups than the native peptide and could bind better aluminium ions. In addition, hydroxyl groups can induce the formation of hydrogen bonds that could lead to the aggregation and fibrillation of free serine peptides.

Second, the $A\beta_{(9-16)}$ peptide fragment and its three analogues, namely $A\beta_{(9-16)}G_{1^{10}}$ ($H^{-9}GGEVHHQK^{16}-NH_2$), $A\beta_{(9-16)}G_{2^{13,14}}$ ($H^{-9}GYEVGGQK^{16}-NH_2$), and $A\beta_{(9-16)}G_{3^{10,13,14}}$ ($H^{-9}GGEVGGQK^{16}-NH_2$), were manually synthesised on a Rink amide resin as solid support using the same fluorenylmethoxycarbonyl chemistry. The resulting crude peptides were purified by RP-HPLC chromatography on a C18 column. Here, Figure 1 refers only to the characterisation with an electrospray ionisation (ESI) ion trap mass spectrometer of the $A\beta_{(1-16)}$ peptide, but all the other peptides used in our experiments were measured by the same procedure (not shown).

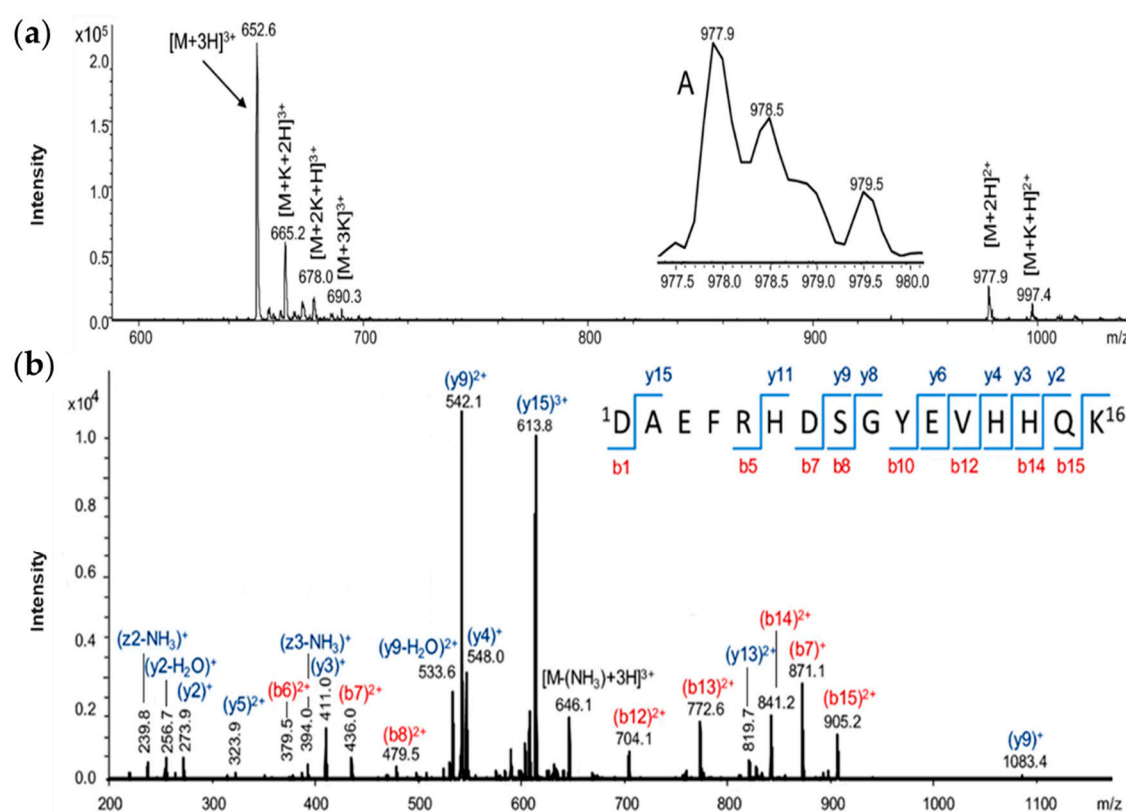


Figure 1. (a) Electrospray ionisation mass spectrometry (ESI-MS) analysis of $A\beta_{(1-16)}$; (b) MS/MS spectrum of $[M + 3H]^{3+}$ molecular ion.

In the ESI ion trap mass spectrum of the $A\beta_{(1-16)}$ peptide (Figure 1a), the most intense signal observed at 652.1 *m/z* was attributed to the triple-charged ion $[M + 3H]^{3+}$, while the low-intensity signal from 977.3 *m/z* was assigned to the double-charged ion $[M + 2H]^{2+}$. In addition, double-charged ions of potassium adduct $[M + K + H]^{2+}$ were noticed at *m/z* 997.4 and the triple-charged one $[M + K + 2H]^{3+}$ was present at *m/z* 665.2 in the mass spectrum. Other potassium-containing molecular ions such as $[M + 2K + H]^{3+}$ and $[M + 3K]^{3+}$ were found at *m/z* 678.0 and *m/z* 690.3. While a simple mass

spectrometer determines the mass of a molecular ion based on the mass/electric charge ratio, tandem mass spectrometry (MS/MS) is used to select a particular molecular ion to determine the mass of the resulting fragment ions and a certain fragmentation pattern. If a molecular ion of a metal complex is fragmented, the fragment containing the metal ion can be stabilised and coordination sites can be determined by collision-induced dissociation (CID). The structure of $A\beta_{(1-16)}$ was also investigated by tandem mass spectrometry (MS/MS), based on a collision-induced dissociation process [32]. The most intense peak in the mass spectrum, belonging to the $[M + 3H]^{3+}$ ion, was selected and subjected to MS/MS fragmentation (Figure 1b). The two intense peaks from m/z 542.1 and m/z 613.8 were assigned to the y -type fragments (y_9^{2+} and y_{15}^{3+}). This type of fragmentation indicated the reduced stability of the peptide bond between the aspartic acid and alanine as well as serine residues. The presence of such peaks in the MS/MS spectra of peptides and their modification in the spectra of aluminium complexes of the investigated peptides may suggest not only the binding site of the metal ion, but also its influence upon the fragmentation mechanism in the CID process. Obviously, the MS/MS spectrum of $A\beta_{(1-16)}$ peptides contains mono-charged ions such as y_2^+ (at m/z 273.9), y_3^+ (m/z 411.0), b_7^+ (m/z 871.1), or y_9^+ (m/z 1083.4). Among the double-positively charged fragments, fragments like y_5^{2+} (m/z 323.9), b_6^{2+} (m/z 379.5), b_7^{2+} (m/z 436.0), b_8^{2+} (m/z 479.5), b_{12}^{2+} (m/z 704.1), b_{13}^{2+} (m/z 772.6), b_{14}^{2+} (m/z 841.2), and b_{15}^{2+} (m/z 905.2) were identified. Some unusual fragments also appeared in the mass spectrum, such as $[y_9-H_2O]^{2+}$ at m/z 533.6, resulting from water removal or ammonia at m/z 646.1 for the $[M-(NH_3)+3H]^{3+}$ ion, m/z 239.8 ($z_2-NH_3^+$), and another at m/z 394 attributed to the ($z_3-NH_3^+$) ion. The unusual peaks were specific to the amidated C-terminal, the $-CONH_2$ group being prone to dehydration by the loss of a water molecule and the formation of a $-CN$ functional group.

The investigation of the MS/MS spectrum of a shorter peptide such as the $A\beta_{(9-16)}$ peptide fragment revealed a wealth of information about its structure. Typical ion fragments that may result from collision-induced dissociation are exemplified in Figure 2. The MS/MS spectrum in Figure 3 shows that the fragmentation occurred mainly in histidine residues; the highest peak was attributed to the y_3^+ fragment resulting from the division of the two histidine residues. In addition, the y_4^+ fragment visible at m/z 548.5 showed a rupture of the peptide bond between histidine and valine. However, while the presence of a b_5^+ fragment ion confirms that the peptide bond between the two histidine residues can be broken, the relatively intense peaks of the b_6^+ and b_7^+ fragment ions may explain the formation of HQ and HH fragments. The m/z values calculated with GPMW software confirmed both the structure and the stability of the peptide molecule.

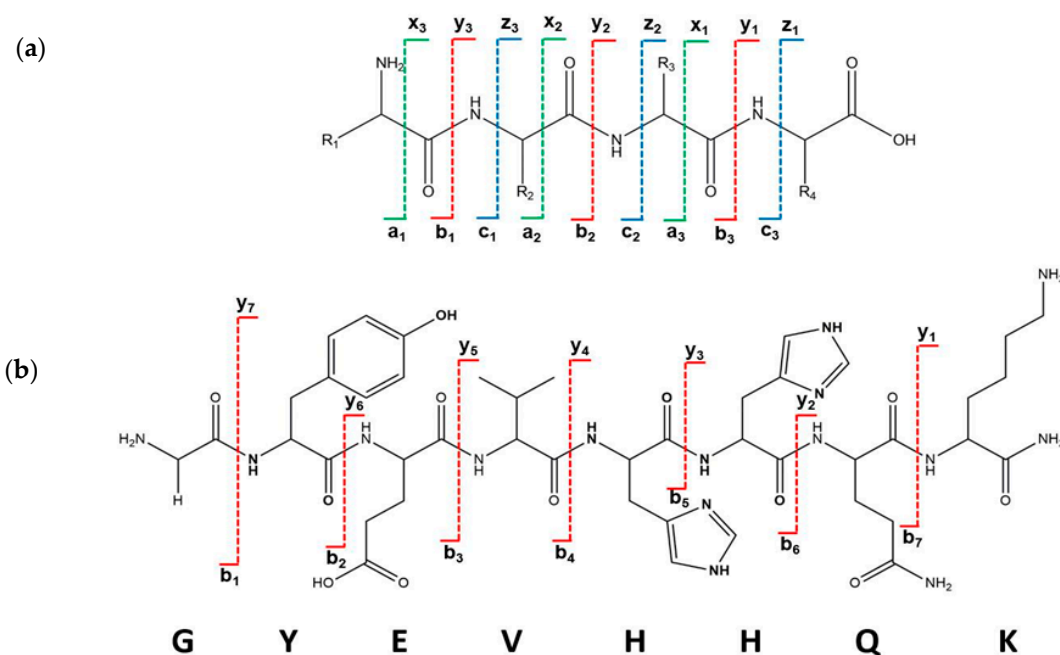


Figure 2. (a) Possible ion fragments which result in the collision-induced dissociation of the $A\beta_{(9-16)}$ peptide, of which some may appear in the MS/MS spectra; (b) the structure of *b*- and *y*-type fragment ions of the GYEVHHQK-NH₂ peptide.

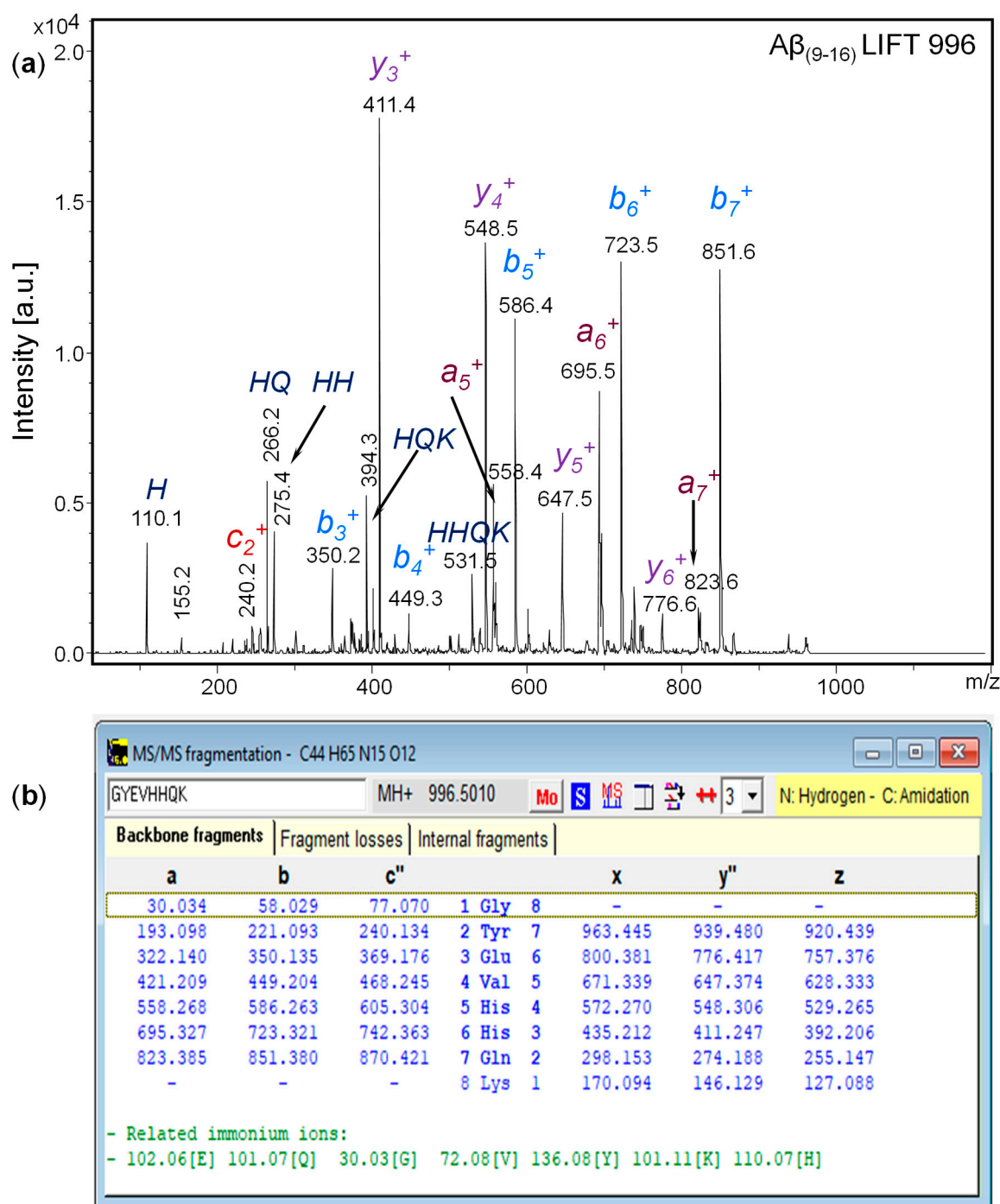


Figure 3. MS/MS fragmentation of free $A\beta_{(9-16)}$ peptide: (a) MS/MS spectrum of amidated $A\beta_{(9-16)}$ peptide; (b) theoretical calculation using GPMW software of *m/z* values of the resulting fragments within the collision-induced dissociation.

2.2. CD Spectroscopy of $A\beta_{(9-16)}$ Peptide Fragment

We started several CD experiments a long time ago to prove conformational changes of peptides upon metal binding. Figure 4 shows the moderately modified CD spectrum of $A\beta_{(9-16)}$ upon the addition of Al³⁺ ions at pH 7.4. The free $A\beta_{(9-16)}$ peptide showed a CD spectrum characterised by two positive absorption bands at 184 nm (89,384 deg·cm²·dmole⁻¹) and 226 nm (17,214 deg·cm²·dmole⁻¹),

as well as a negative absorption band at 193–197 nm ($132,353 \text{ deg cm}^2 \text{ dmole}^{-1}$). The shape of the $A\beta_{(9-16)}$ CD spectrum suggested rather a random coil conformation of this small peptide, especially due to the presence of a minimum at about 197 nm. In addition, the solution of pure $A\beta_{(9-16)}$ may have a significant proportion of α -helical conformers, as suggested by the positive maximum at 184 nm. However, a full helical protein has a maximum shifted to 191–193 nm in the CD spectrum. The profile of the $A\beta_{(9-16)}$ far-UV CD spectrum was much changed in the presence of Al^{3+} ions at a 1:1 molar ratio. We thus suspected a certain increase in the proportion of β -turn populations following the addition of Al^{3+} ions. Besides, the spectrum appears to have characteristics closer to those of an α -helix-like spectrum. Nevertheless, the strong double minimum was found at 191.5 nm ($65,138 \text{ deg cm}^2 \text{ dmole}^{-1}$) and 197.5 nm ($67,925 \text{ deg cm}^2 \text{ dmole}^{-1}$), and not at 208 and 222 nm, as the case of total α -helical conformers. On using Dicroprot software of the CD instrument, the free peptide had the following proportions of conformers: 0% α -helix, 25.66% β -sheet, 22.23% β -turn, and 52.11% random coil. Upon aluminium addition, these proportions slightly changed (3.34% α -helix, 24.88% β -sheet, 22.84% β -turn, and 48.94% random coil).

We thus hypothesised that because the samples of $A\beta_{(9-16)}$ were dissolved in an ammonium acetate buffer (15 mM) at pH 7.4, the aluminium ions bound very weakly to the peptide backbone and, as a result, the peptide conformation was only slightly altered. Therefore, we designed new experiments with $A\beta_{(9-16)}$ and its analogues at a lower pH value (pH 6.6).

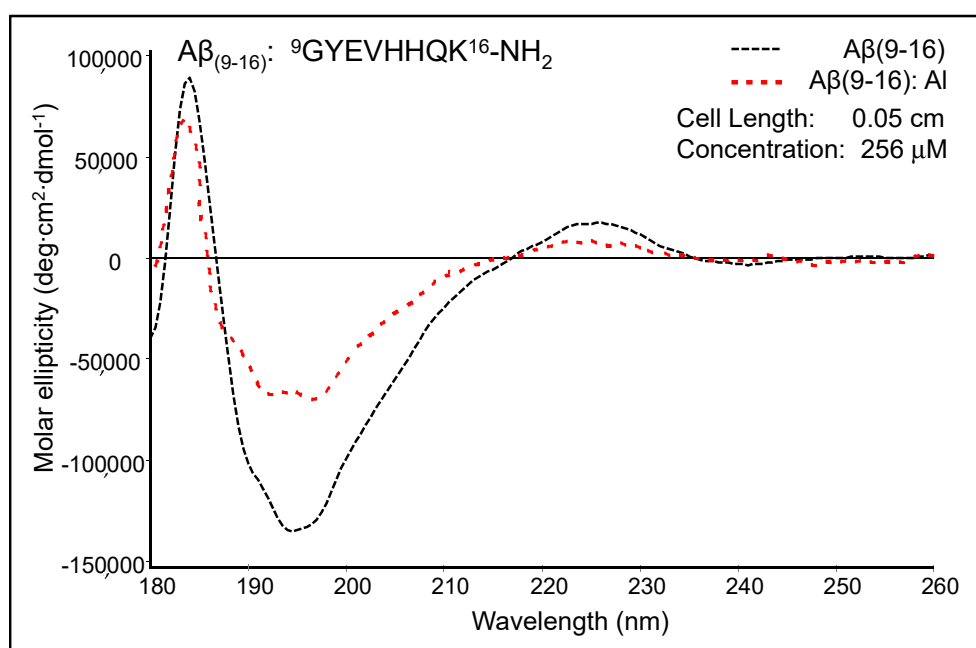


Figure 4. The effect of aluminium ions on the circular dichroism (CD) spectrum of $A\beta_{(9-16)}$ peptide (pH 7.4; 1:1 $Al:A\beta_{(9-16)}$ peptide molar ratio).

2.3. Interaction of $A\beta_{(9-16)}$ Peptide and Its Analogues with Al Ions at pH 6.6

The aluminium may have had a higher affinity to amyloid peptides at a lower pH due to the reaction of this metal with acidic residues in the peptide sequences. Here, the existence of Al–peptide complexes was highlighted by MS measurements. The experimental values were then compared with those calculated theoretically. Mass spectra unequivocally showed the formation of aluminium complexes of $A\beta_{(9-16)}$ peptides of the formula $[M + Al - 2H]^+$, where M is $A\beta_{(9-16)}$, $A\beta_{(9-16)}G_{10}$, $A\beta_{(9-16)}G_{213,14}$, and $A\beta_{(9-16)}G_{310,13,14}$. It is thought that the binding capacity of aluminium ions is closely related to the toxicity of amyloid peptides, with high concentrations of aluminium being found in senile plaques [35]. Thus, determining how the metal ion binds to the amyloid fragment, together with the study of conformational changes undergone by peptides in the presence of aluminium, could provide important information for understanding AD pathology. Here, both the $A\beta_{(9-16)}$ fragment and its analogues produced by replacing tyrosine and histidine residues with glycine ($A\beta_{(9-16)}G_{10}$, $A\beta_{(9-16)}$

$G_{2^{13,14}}$, and $A\beta_{(9-16)}G_{3^{10,13,14}}$) were analysed by MALDI-ToF mass spectrometry in the absence and in the presence of aluminium ions.

Figure 5a presents the mass spectra of peptides recorded in the absence of aluminium ions, while the interaction with metal ions can be noticed in Figure 5b. The juxtaposition of these spectra allows for the assessment of interactions between the studied peptides and aluminium ions. The free peptides generated several peaks attributed to the molecular ions of the protonated peptide $[M + H]^+$, as well as to the adducts with sodium $[M + Na]^+$ and potassium $[M + K]^+$. The presence of aluminium ions led to the formation of a peptide–metal complex that generated molecular ions of the $[M + Al - 2H]^+$ type. However, the peaks of sodium and potassium adducts of all peptides disappeared in the MS spectrum taken in the presence of aluminium chloride, suggesting that these ions were replaced by Al ions. Although MALDI-ToF MS measurements cannot estimate the proportion of peptide molecules bound to metal ions, the peak intensity of the aluminium complexes suggests that the $A\beta_{(9-16)}$ peptide had a considerable affinity to Al ions (intensity ratio $[M + Al - 2H]^+ / [M + H]^+ = 31.39\%$). At the same time, the highest intensity ratio was calculated for $A\beta_{(9-16)}G_{2^{13,14}}$ (50.45%), whereas the lowest was that of the $A\beta_{(9-16)}G_{3^{10,13,14}}$ peptide (20.68%). These findings suggest that the glycine-induced molecule flexibility could play an important role in Al binding. In addition, they confirm that histidine residues cannot be bound to Al.

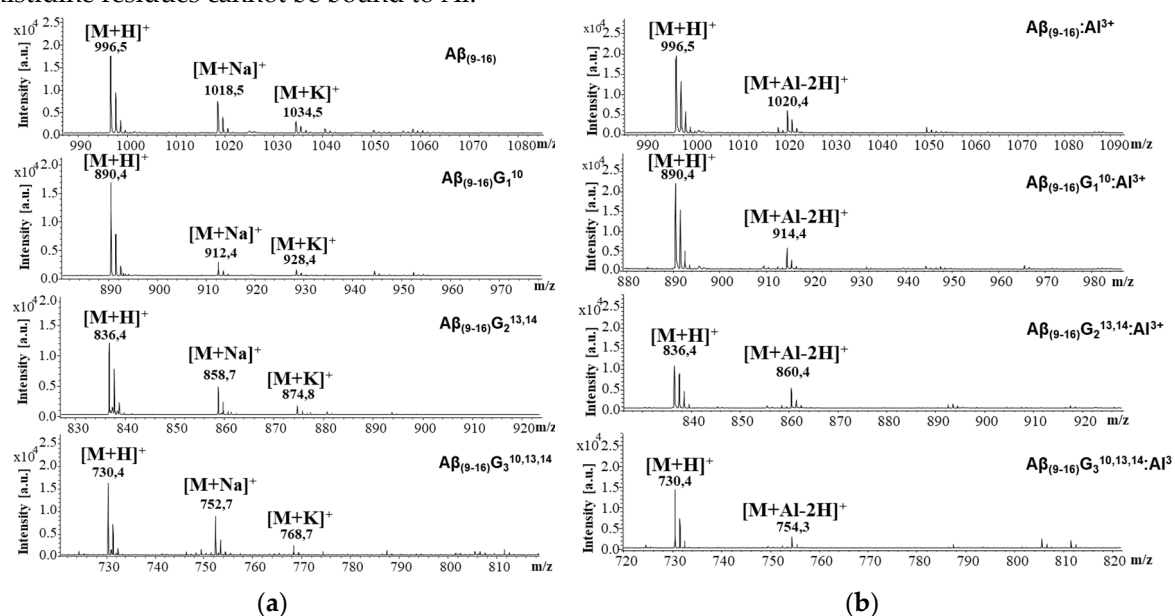


Figure 5. Matrix-assisted laser desorption ionization time-of-flight mass spectrometry (MALDI-ToF MS) analysis of (a) $A\beta_{(9-16)}$ peptide (GYEVHHQK-NH₂) and its glycine analogues: $A\beta_{(9-16)}G_{1^{10}}$ (GGEVHHQK-NH₂), $A\beta_{(9-16)}G_{2^{13,14}}$ (GYEVGGQK-NH₂), and $A\beta_{(9-16)}G_{3^{10,13,14}}$ (GGEVGGQK-NH₂); (b) MALDI-ToF MS spectra of $A\beta_{(9-16)}$ peptides in the presence of aluminium ions (AlCl₃).

Before fragmenting the peak of the $[M + Al - 2H]^+$ complex, we studied the fragmentation of the peptide molecules in order to compare the resulting ions (Figure 6). The MS/MS spectra showed that the four $A\beta_{(9-16)}$ peptides differ greatly in the type and intensity of the fragments resulting from the CID process. Thus, in the spectrum of $A\beta_{(9-16)}$ peptides and that of tyrosine-free peptides, $A\beta_{(9-16)}G_{1^{10}}$, the y_3^+ fragment (at m/z 411.4 and 411.7) afforded the most intense peaks, while the fragment y_4^+ of glycine-rich peptides ($A\beta_{(9-16)}G_{2^{13,14}}$ and $A\beta_{(9-16)}G_{3^{10,13,14}}$) had the highest intensity. In addition, the order of peak intensity was as follows: $A\beta_{(9-16)}$, $y_3^+ > y_4^+ > b_6^+ > b_7^+$; $A\beta_{(9-16)}G_{1^{10}}$, $y_3^+ > b_6^+ > b_5^+ > b_7^+$; $A\beta_{(9-16)}G_{2^{13,14}}$, $y_4^+ > b_3^+ > y_5^+ > z_1^+$; $A\beta_{(9-16)}G_{3^{10,13,14}}$, $y_4^+ > b_3^+ > z_1^+ > y_5^+$.

Following MS experiments with the Al–peptide complexes, we selected the parent ion $[M + Al - 2H]^+$ and subjected it to CID fragmentation. The assignment of the signals observed in the MS/MS spectra of $[M + Al - 2H]^+$ ions was performed by comparing the theoretical molecular masses of the ions resulting from the CID fragmentation with the experimentally recorded values. The experimentally determined m/z values were in accordance with the theoretical values. A comparison

of the theoretical m/z values estimated using GPMW software with the experimental data can be seen in Table 1.

Table 1. The m/z values calculated and measured experimentally using MS/MS spectra of ions $[M+Al(III)-2H]^+$ following the collision-induced dissociation (CID) fragmentation (MALDI mass spectrometer).

Peptide	Sequence	Theoretical (m/z)	Experimental (m/z)
$A\beta_{(9-16)}$ GYEVHHQK	H	110.0	110.1
	b_4 -NH ₂	433.2	433.3
	VHHQ	502.2	502.3
	b_5 -NH ₂	570.2	570.4
	a_5 + Al (a_5 + Al - 3H)	582.2	582.2
	b_5 + Al (b_5 + Al - 3H)	610.2	610.3
	y_5 + Al (y_5 + Al - 3H)	671.3	671.5
	a_6 + Al (a_6 + Al - 3H)	719.3	719.4
	b_6 + Al (b_6 + Al - 3H)	747.3	747.5
	x_6 + Al (x_6 + Al - 3H)	824.3	824.0
$A\beta_{(9-16)}G_1^{10}$ GGEVHHQK	a_7 + Al (a_7 + Al - 3H)	847.3	847.6
	H	110.0	110.2
	c2	134.0	134.2
	HQ	266.1	266.2
	a_5 -H ₂ O	434.2	433.4
	y_4 + Al (y_4 + Al - 3H)	572.3	572.6
	a_6 + Al (a_6 + Al - 3H)	613.2	613.6
	b_6 + Al (b_6 + Al - 3H)	641.2	641.6
	y_5 + Al (y_5 + Al - 3H)	671.3	670.7
	a_7 + Al (a_7 + Al - 3H)	741.3	741.8
$A\beta_{(9-16)}G_2^{13,14}$ GYEVGGQK	y_4 + Al (y_4 + Al - 3H)	412.2	411.6
	c5-NH ₂	509.2	509.7
$A\beta_{(9-16)}G_3^{10,13,14}$ GGEVGGQK	VGGQ	342.1	342.3
	y_5 + Al (y_5 + Al - 3H)	511.2	510.7
	z7	654.3	654.7

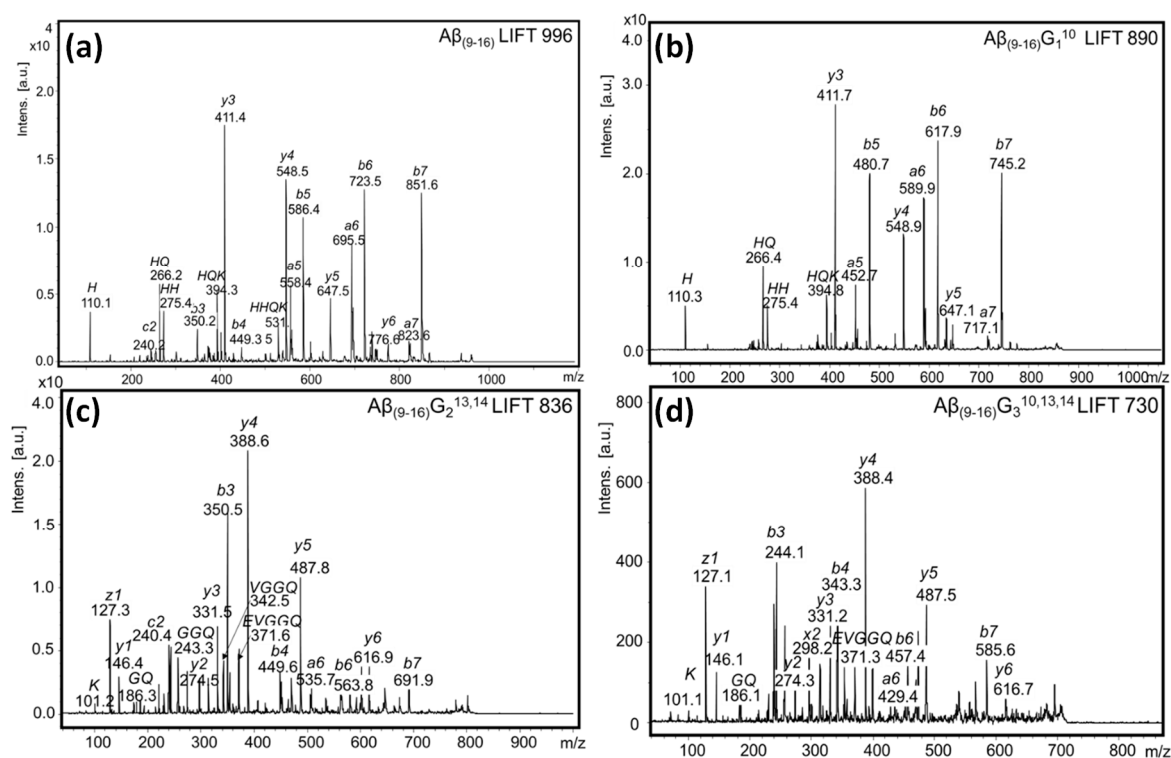
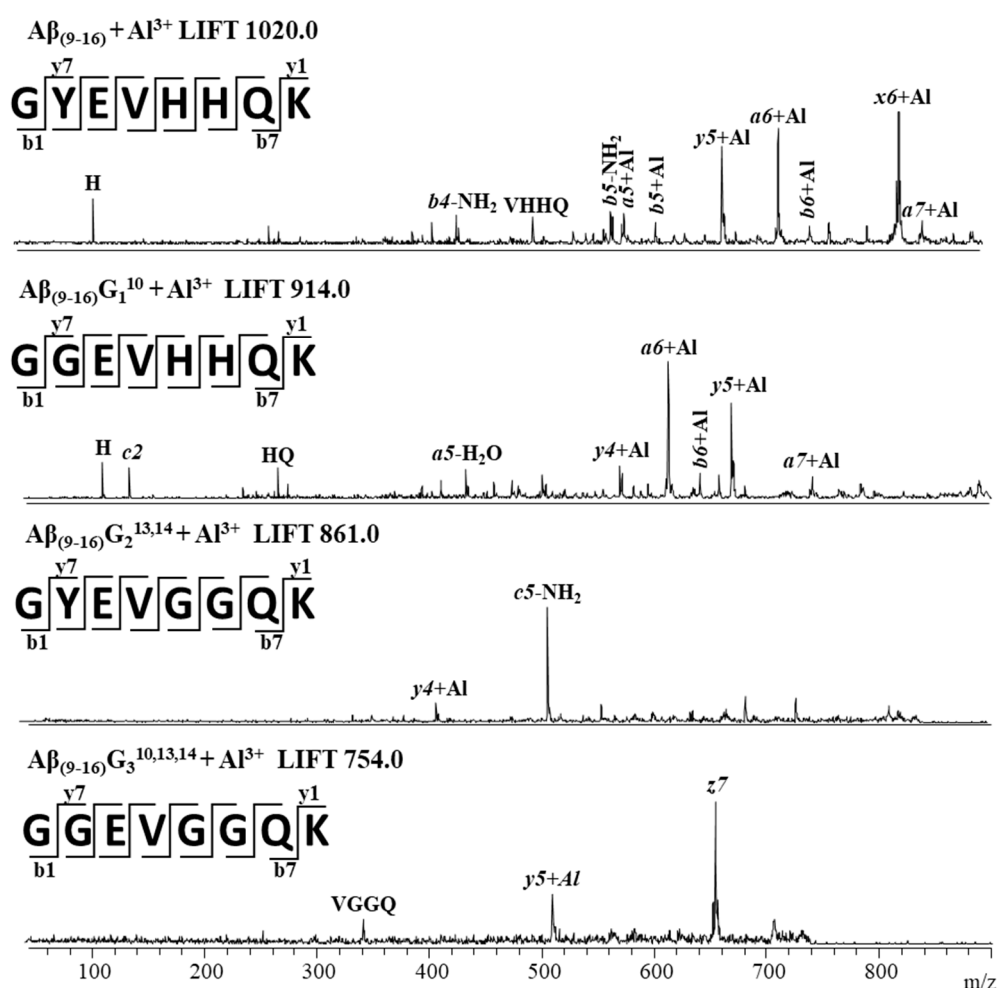


Figure 6. MS/MS spectra of the modified $A\beta_{(9-16)}$ peptides: (a) $A\beta_{(9-16)}$; (b) $A\beta_{(9-16)}G_1^{10}$; (c) $A\beta_{(9-16)}G_2^{13,14}$; (d) $A\beta_{(9-16)}G_3^{10,13,14}$.

$A\beta_{(9-16)}$ peptides, containing two histidine residues in the molecule, generated numerous peaks, most of them bound to Al ions, such as $[Al + x_6^+ - 3H]^+$, $[Al + a_6^+ - 3H]^+$, $[Al + y_5^+ - 3H]^+$, $[Al + a_5^+ - 3H]^+$, and $[Al + b_5^+ - 3H]^+$ (Figure 7). Only a few peaks were assigned to peptide fragment ions without aluminium. The $A\beta_{(9-16)}G_1^{10}$ peptide, obtained by replacing the tyrosine residue with glycine, also had many peaks in the MS/MS spectrum, which were attributed to Al-containing peptide fragment ions such as $[Al + a_6^+ - 3H]^+$, $[Al + y_5^+ - 3H]^+$, $[Al + y_4^+ - 3H]^+$, $[Al + b_6^+ - 3H]^+$, and $[Al + a_7^+ - 3H]^+$, suggesting that aluminium protected the peptide bond between the two histidine residues. In addition, while the fragmentation of the free peptides occurred mainly at the peptide bond between the histidine residues to form the y_3^+ fragment, Al induced different fragmentation to generate the a -type fragments containing metal ions.

As for the glycine-enriched peptides, only the y_4^+ and y_5^+ fragment ions were found to possess Al bound to their backbone, which suggests a weaker interaction of these peptides with Al ions. Besides, the presence of $[b_4-NH_2]^+$ and $[b_5-NH_2]^+$ structures was noticed in the MS/MS spectrum of the $A\beta_{(9-16)}$ peptide and $[c_5-NH_2]^+$ in that of the $A\beta_{(9-16)}G_2^{13,14}$ peptide, which suggests a possible cyclisation followed by removing the NH_2 radical induced by Al. The main peak in the MS/MS spectrum of the $A\beta_{(9-16)}G_3^{10,13,14}$ peptide was assigned to z_7^+ , while this fragment does not appear in the spectrum of free peptides. This may be evidence that the binding of Al to the investigated peptides changed their stability and induced different fragmentation patterns. Although aluminium ions may be not capable of binding to the histidine residues of $A\beta$ peptides, they can bind easily to HHQK peptide fragments and less well to GYEV or GGEV residues. However, glycine residues in the modified $A\beta_{(9-16)}$ peptides induce a high degree of flexibility, which may inhibit Al binding to peptides.



stretching vibrations of the CH_3 group, of the deformation in the plane of the CH_2 group, and of the stretching of the CN bond underwent a partial division that led to the appearance of several peaks.

In the interval of $1500\text{--}1700\text{ cm}^{-1}$, specific to the amide I and amide II bonds, the aluminium ions determined a partial overlap of the two absorption maxima. Specifically, the maximum values recorded in the spectra of the $\text{A}\beta_{(9-16)}$ peptides (1538 cm^{-1}) in the presence of metal ions were attributed to disordered structures, the influence of β -conformation folding observed in the spectra of free peptides being much diminished. Similar changes were observed in the case of glycine-enriched peptides ($\text{A}\beta_{(9-16)}\text{G}_1^{10}$, $\text{A}\beta_{(9-16)}\text{G}_2^{13,14}$, and $\text{A}\beta_{(9-16)}\text{G}_3^{10,13,14}$), where the presence of aluminium favoured the adoption of rather disordered structures, but α -helix and β -sheet conformers may also have been present. Nevertheless, it was difficult to see the presence of all types of conformers among the small peptide molecules from the FT-IR spectra.

Structural changes were also identified in the amide I domain, where the signal displayed in the spectra of peptides incubated with Al^{3+} ions showed a single maximum value, which suggested a β -folded structure (1631 cm^{-1} , 1634 cm^{-1} , and 1637 cm^{-1}), unlike the spectra of free peptides, which suggested mainly α -helical conformations ($\text{A}\beta_{(9-16)}\text{G}_2^{13,14}$ and $\text{A}\beta_{(9-16)}\text{G}_3^{10,13,14}$).

Figure 9 shows the spectra of second-order derivatives of amyloid peptides in the absence and presence of aluminium ions. The calculation of the derivative made it possible to obtain more accurate information in the amide I region on the conformations adopted by the peptides. Although the β -folded structure of the peptides $\text{A}\beta_{(9-16)}$ and $\text{A}\beta_{(9-16)}\text{G}_1^{10}$ was also present when they were treated with AlCl_3 , by generating signals in the $1639\text{--}1630\text{ cm}^{-1}$ region, the most important result was the intense bands with maxima at $1612\text{--}1613\text{ cm}^{-1}$, attributed to an aggregate-type structure (Figure 9b). However, the α -helical conformation was evidenced in the structure of the peptides $\text{A}\beta_{(9-16)}\text{G}_2^{13,14}$ and $\text{A}\beta_{(9-16)}\text{G}_3^{10,13,14}$ in samples incubated with Al ions (1650 cm^{-1} and 1651 cm^{-1}).

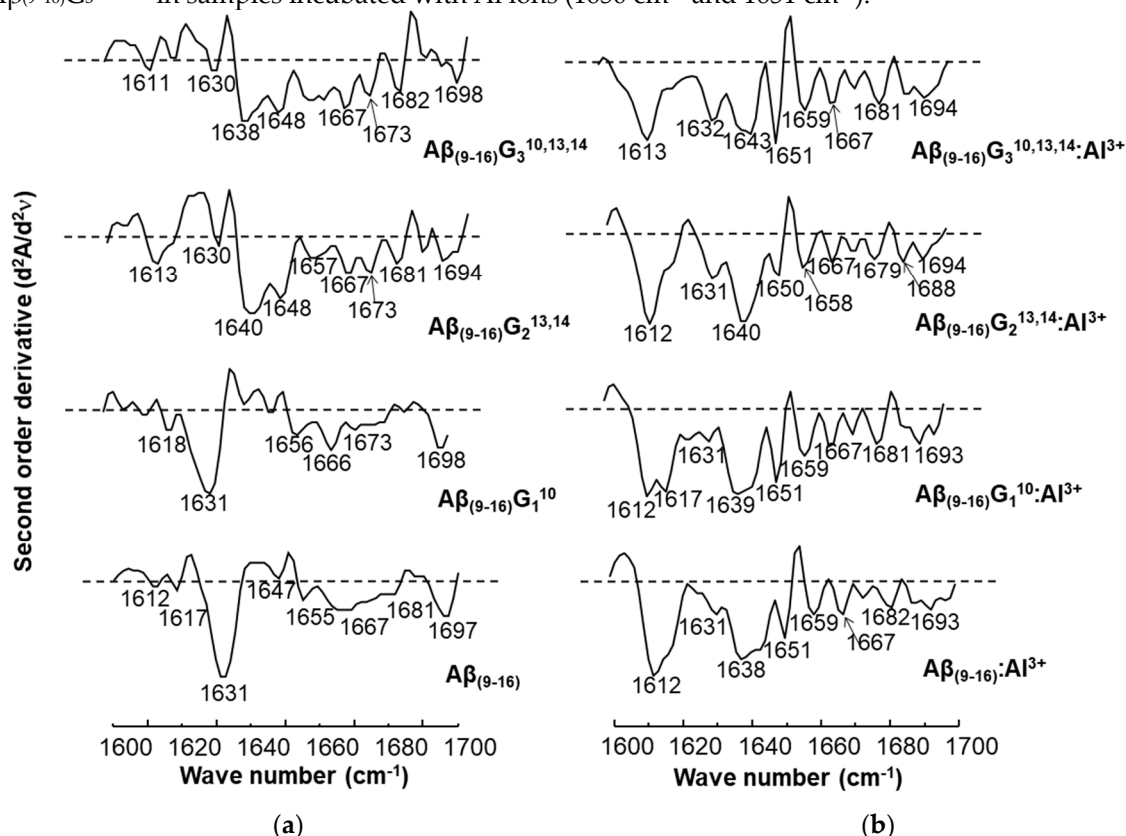


Figure 9. Second-order derivatives of the FT-IR spectra of amyloid peptides calculated in the range $1600\text{--}1700\text{ cm}^{-1}$: (a) in the absence of aluminium ions; (b) in the presence of aluminium ions.

2.5. $\text{A}\beta_{1-16}$ Conformational Changes Induced by Aluminium Ions

2.5.1. Atomic Force Microscopy

AFM images showed that peptide assemblies have different two-dimensional layer-shaped structures (Figure 10). A solution of free $A\beta_{(1-16)}$ peptides produced a smooth film and no fibrils or aggregates were evident on the glass plate of the microscope. We assumed that its low tendency to aggregation is related to the hydrophilic N-terminus sequence of amyloid- β peptides. On the contrary, the alanine-rich $A\beta_{(1-16)}$ peptide formed fibrils, most probably due to its hydrophobic characteristic, while serine-rich peptides had a pronounced tendency to fibrillation due to hydrogen bonding of serine residues. Thus, by replacing the histidine residues with alanine in the native $A\beta_{(1-16)}$ sequence, a texture composed of differently sized fibrils appeared. Some fibrils were about 80–100 nm thick and more than 0.5 μm long, whereas the other ones were smaller but also in the nanometre range. We supposed that alanine residues highly increased the peptide hydrophobicity, as well as its α -helical proportion, thus making possible the association of molecules through non-covalent interactions. Serine-rich $A\beta_{(1-16)}$ peptides generated even larger fibrils and aggregates. This phenomenon could be possible due to the intermolecular hydrogen bonds.

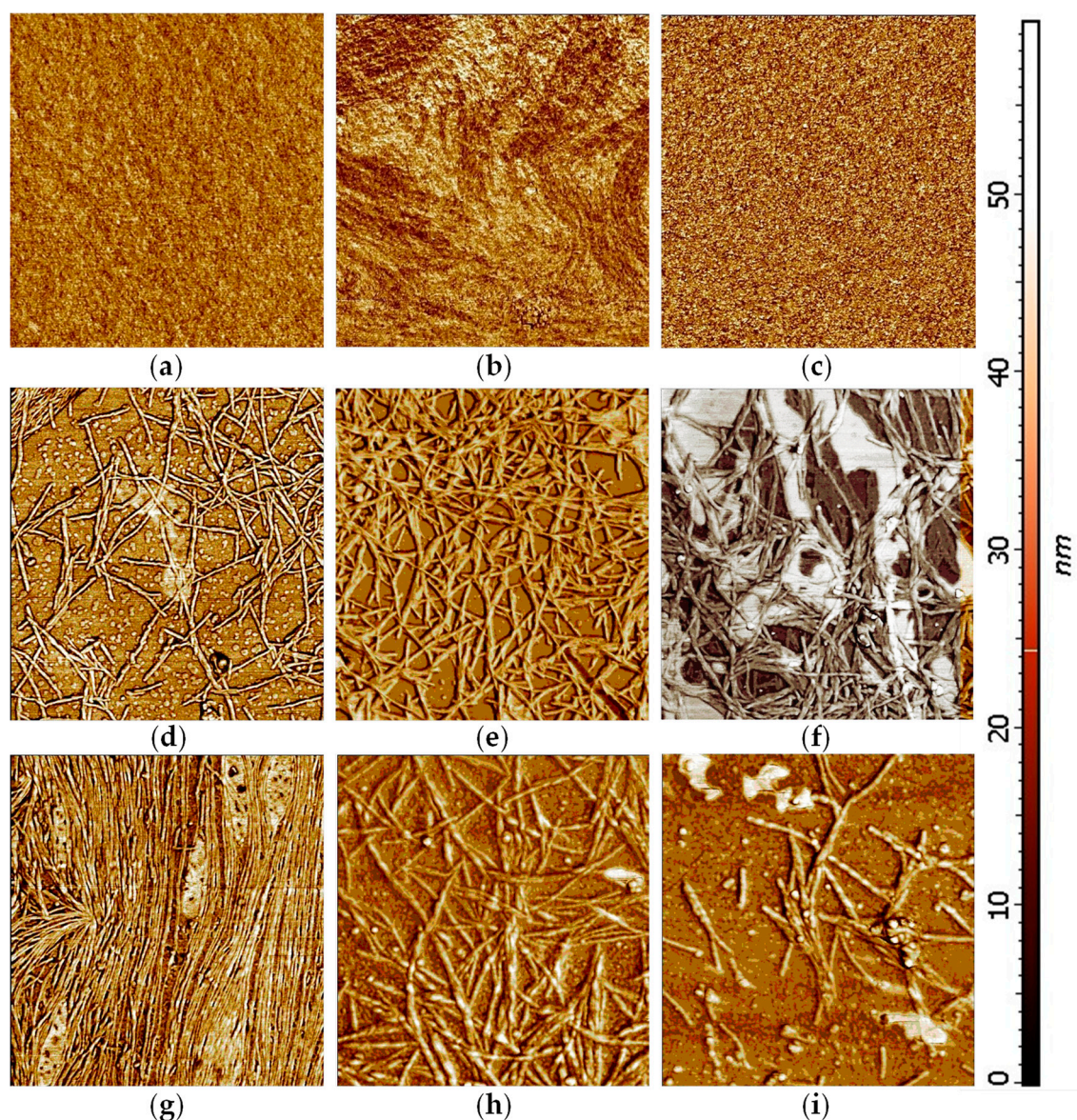


Figure 10. Atomic force microscopy (AFM) images of film surfaces of peptide complexes with aluminium ions. (a) Free $A\beta_{(1-16)}$; (b) $A\beta_{(1-16)} + \text{Al}_2(\text{SO}_4)_3$, 1:1 molar ratio; (c) $A\beta_{(1-16)} + \text{Al}_2(\text{SO}_4)_3$, 1:2 molar ratio; (d) free $A\beta_{(1-16)}A_{3^6,13,14}$; (e) $A\beta_{(1-16)}A_{3^6,13,14} + \text{Al}_2(\text{SO}_4)_3$, 1:1 molar ratio; (f) $A\beta_{(1-16)}A_{3^6,13,14} + \text{Al}_2(\text{SO}_4)_3$, 1:2 molar ratio; (g) free $A\beta_{(1-16)}S_{3^6,13,14}$; (h) $A\beta_{(1-16)}S_{3^6,13,14} + \text{Al}_2(\text{SO}_4)_3$, 1:1 molar ratio; (i) $A\beta_{(1-16)}S_{3^6,13,14} + \text{Al}_2(\text{SO}_4)_3$, 1:2 molar ratio (peptide concentration: 256 μM ; image size: $2 \times 2 \mu\text{m}$).

In brief, AFM images, as well as CD and FT-IR spectra, showed that the $A\beta_{(1-16)}$ peptide conformation and fibrillation depend on the peptide sequence and the presence of aluminium in solution. The film surface of the native peptide $A\beta_{(1-16)}$ changed only slightly with the addition of aluminum at pH 6.6 (Figure 9b,c). Aluminium ions induced the aggregation and fibrillation of modified peptides as demonstrated by AFM and SEM experiments. Thus, $A\beta_{(1-16)}A_{3^{6,13,14}}$ generated fibrils even in the absence of Al, being a hydrophobic peptide. In the presence of Al sulphate, the fibrils became longer and thicker. The excess of aluminium salt can be observed in the AFM images for the 1:2 peptide:Al ratio. On the contrary, serine-rich peptides can form fibrils due to the hydrogen bonds.

2.5.2. Scanning Electron Microscopy

The interaction of the two modified $A\beta_{(1-16)}$ peptides with aluminium was confirmed by SEM (Figure 11) that showed a rough surface, with fibrils differently and densely distributed. These are genuine indicators of the strong interaction between the peptides and Al. SEM images of free $A\beta_{(1-16)}A_{3^{6,13,14}}$ revealed numerous amyloid fibrils displaying the characteristic twist found in $A\beta$ fibrils (Figure 11a). The modified $A\beta$ peptides formed aggregates characterised by short fibrils which intertwine and appear rigid. With the addition of aluminium ions, the fibrils became more ordered and longer, whereas some of them seem to be finer (Figure 11b). A similar phenomenon seems to occur in the case of the formation of $A\beta_{(1-16)}A_{3^{6,13,14}}$ films in the presence of aluminium ions (Figure 10e,f). As the concentration of metal ions increased, the large fibrils formed (Figure 10e), became longer, and some of them became thinner (Figure 10f). We assumed that Al increased the hydrophobicity of $A\beta_{(1-16)}A_{3^{6,13,14}}$, which led to the formation of thicker and longer fibrils, followed by their division as aluminium sulphate concentration increased. In addition, these fibrils are longer and intertwined. The serine-rich peptides show short, thin fibres, which thickened and lengthened in the presence of aluminium ions (Figure 11c,d).

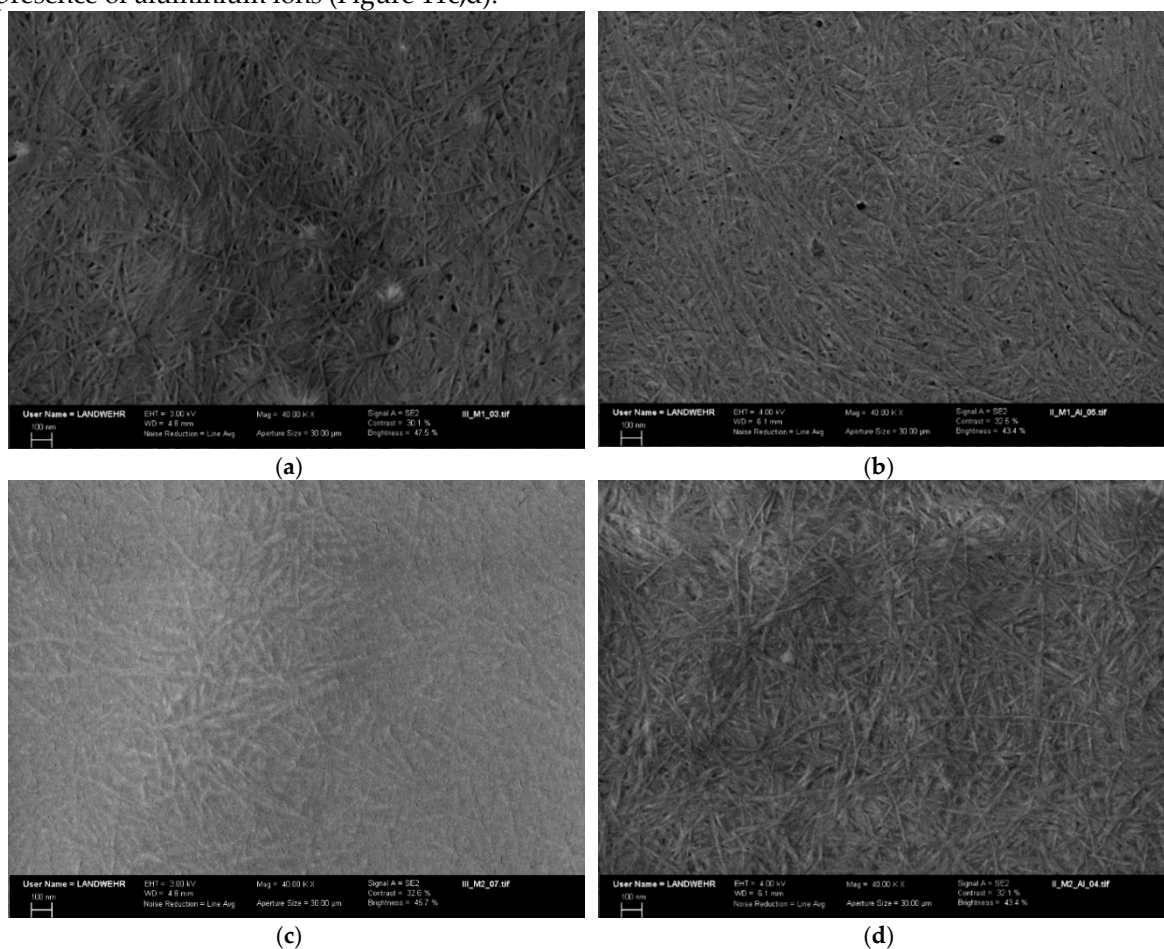


Figure 11. SEM images of (a) $A\beta_{(1-16)}A_{3^{6,13,14}}$; (b) $A\beta_{(1-16)}A_{3^{6,13,14}} + Al^{3+}$; (c) $A\beta_{(1-16)}S_{3^{6,13,14}}$; (d) $A\beta_{(1-16)}S_{3^{6,13,14}} + Al^{3+}$ (mag: 40 KX, aperture size: 30 μm).

2.6. Nuclear Magnetic Resonance Spectroscopy

In the NMR study of the $A\beta_{(1-16)}$ and $A\beta_{(9-16)}$ fragments as well as their analogues, presented here, the interactions of these peptides with aluminium were investigated. Although we found significant changes of 1H -NMR spectra in the presence of aluminium sulphate, we investigate here only the spectra of some very small peptides as models. We were interested in showing that the amino acid residues may be capable of binding to or interacting with aluminium ions in solutions. However, we present here, in Figure 14, some spectra of $A\beta_{(9-16)}$ peptide fragments in deuterium oxide solution, alone, or in the presence of aluminium ions.

Our experiment showed that glycyl-tyrosine bound aluminium ions in the aluminium sulphate aqueous solutions at the peptide bond region and not at the phenolic OH group (Figure 12). Although all the protons were affected by Al, the most influenced were the protons of the tyrosine CH_2 group (the peaks shifted from 3.085–3.123 ppm to 3.125–3.212 ppm, also becoming enlarged) and the protons of the glycine CH_2 group (from 3.630–3.769 ppm to 3.661–3.694 ppm). Of course, the proton near the COOH group was also much affected.

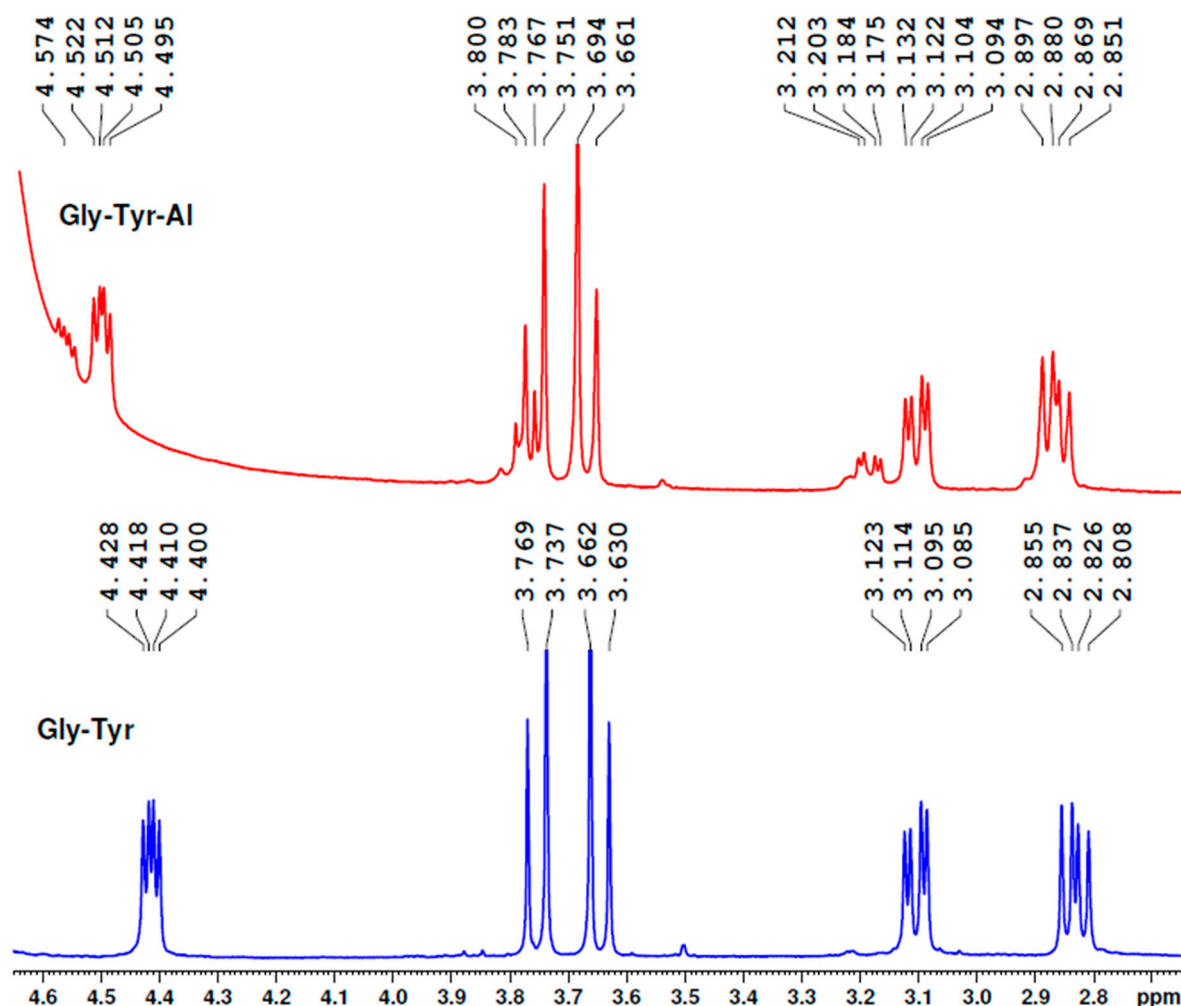


Figure 12. 1H -NMR spectra of glycyl-tyrosine peptide, which demonstrate the influence of Al on the two protons of the tyrosine CH_2 group (3.085–3.123 ppm) and the two protons of the glycine CH_2 group (3.630–3.769 ppm).

The 1H -NMR spectrum of seryl-glycine contains the serine CH_2 protons in the 3.754–3.897 ppm region (Figure 13). Under the influence of Al, we found the peaks shifted to 3.799–3.927 ppm, but the

distance between the highest signals was smaller. These findings demonstrate that aluminium ions are bound to serine OH groups. In addition, the two protons of the glycine CH₂ group were found to be shifted toward higher ppm values and wider. Besides, the CH groups of serine residues bound to amino groups were also modified.

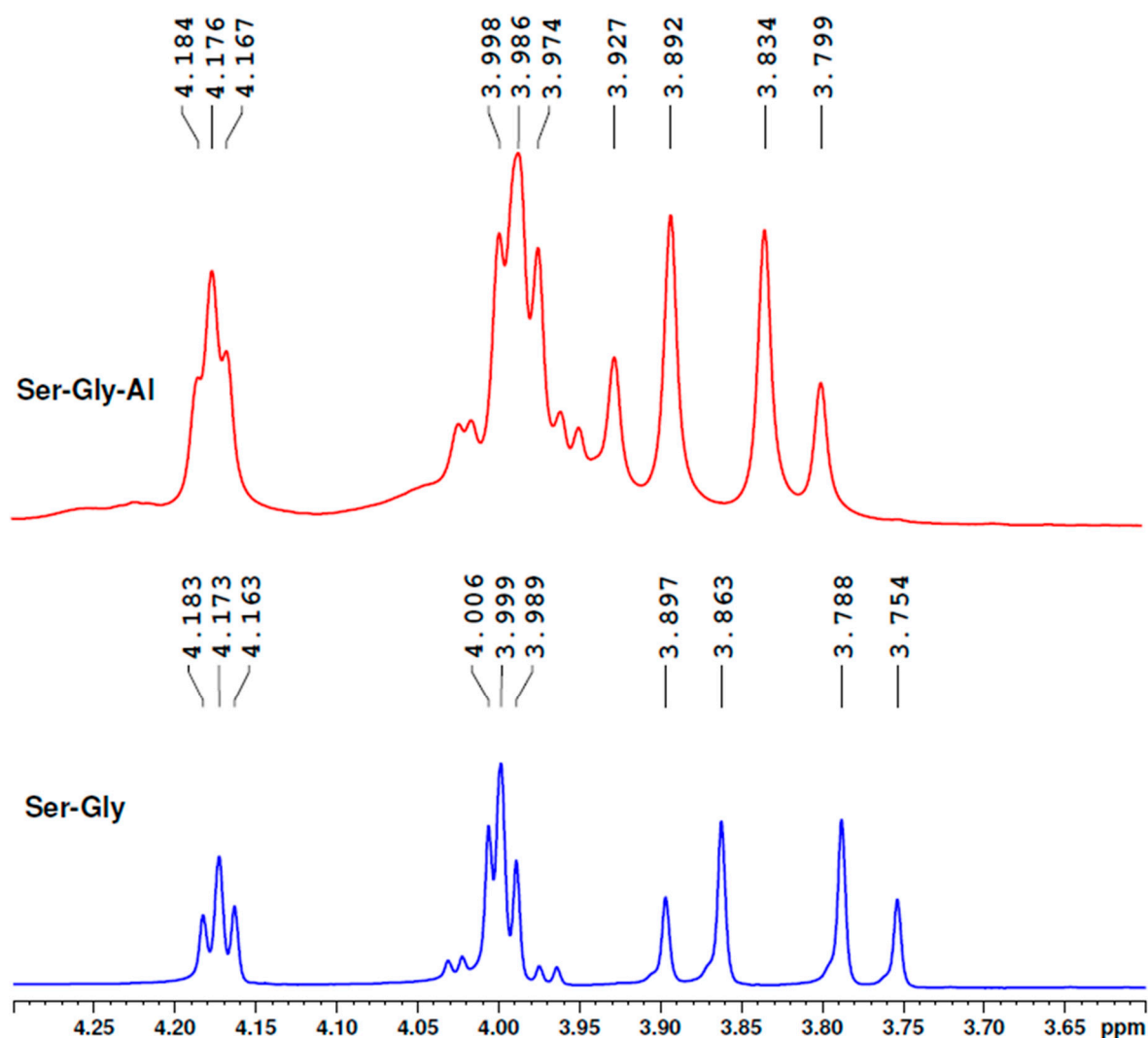


Figure 13. ¹H-NMR spectra of seryl-glycine peptide in the presence of aluminium sulphate demonstrate that Al ions bound to the hydroxyl group of serine.

These data confirm that the peptide backbone is also involved in aluminium binding and the hydroxyl group of serine also binds aluminium ions.

Figure 14 shows that the NMR spectra of the A β _(9–16) peptide is slightly changed in the presence of aluminium ions. However, we also studied by NMR spectroscopy Al binding to A β _(9–16), A β _(1–16), or only its interaction with these peptides, as well as their modified variants, and continued with A β _(1–40) and its variants in which the histidine residues were replaced with serine and alanine ones (not shown). Some other experiments are in progress, in which larger amounts of peptides are used, and, therefore, a new manuscript is expected to disseminate the results.

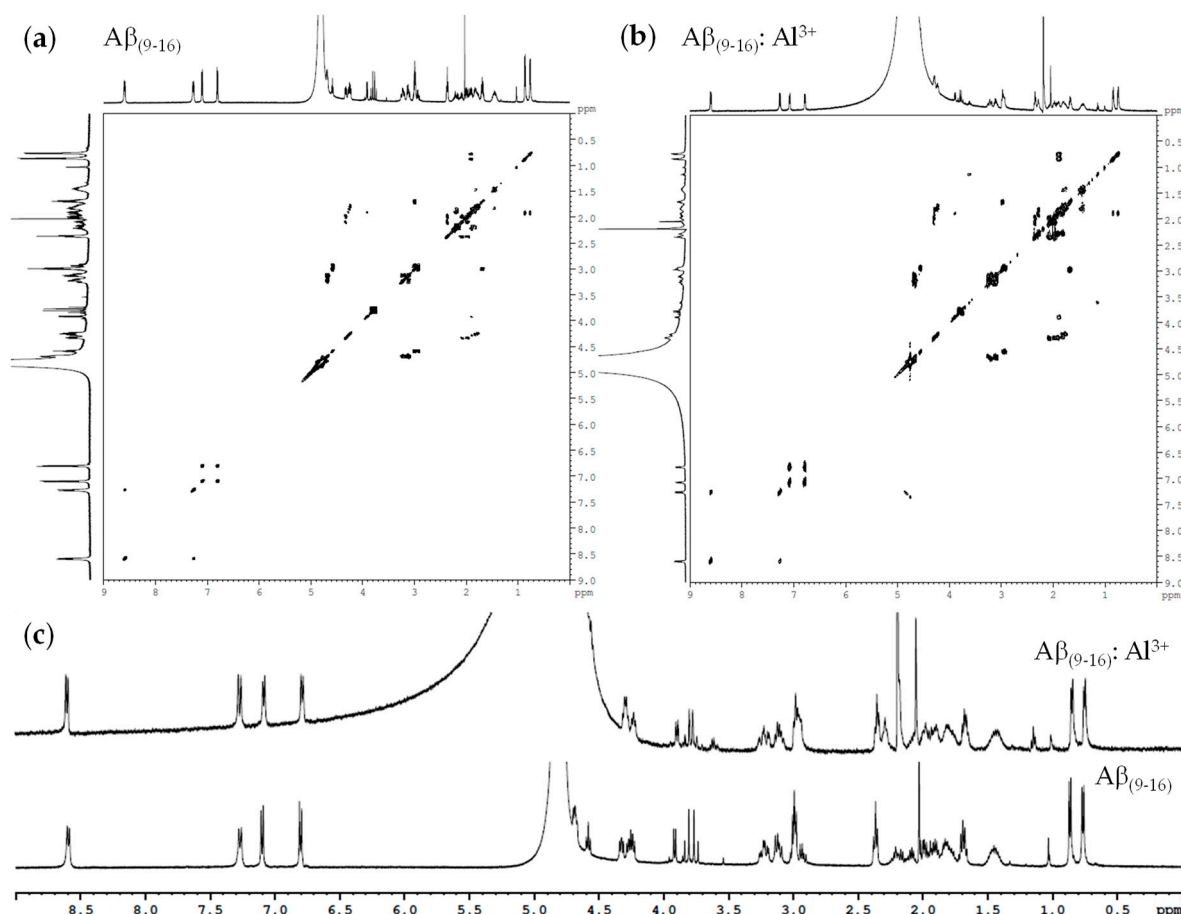


Figure 14. ^1H -NMR spectra of $\text{A}\beta_{(9-16)}$ peptide in the presence of aluminium sulphate: (a) COSY ^1H NMR spectrum of $\text{A}\beta_{(9-16)}$ peptide; (b) COSY ^1H NMR spectrum of $\text{A}\beta_{(9-16)}$ in the presence of Al^{3+} ; (c) ^1H -NMR spectra.

3. Discussion

Interaction of metal ions with $\text{A}\beta$ is mediated mostly by the N-terminal $\text{A}\beta_{(1-16)}$ domain and appears to play an important role in AD progression [36]. Although Al ions also were reported to bind to some residues found in the $\text{A}\beta_{(1-28)}$ sequence, no measurable amounts of $\text{A}\beta_{(1-28)}\text{-Al}^{3+}$ adducts were noticed by other authors within their experiments by ^1H NMR and electrospray ionisation mass spectrometry (ESI-MS) at physiological pH [37]. These were the incentive conditions for the present investigation of Al interactions with $\text{A}\beta$ in which we synthesised several variants of the $\text{A}\beta_{(1-16)}$ and $\text{A}\beta_{(9-16)}$ peptides, and which contain histidine residues replaced by alanine, serine, or glycine. Since the interaction of amyloid- β peptides with Al ions might be involved in AD pathogenesis, we investigated aluminium binding to the newly synthesised peptides by MS, FT-IR, CD, AFM, and NMR spectroscopy.

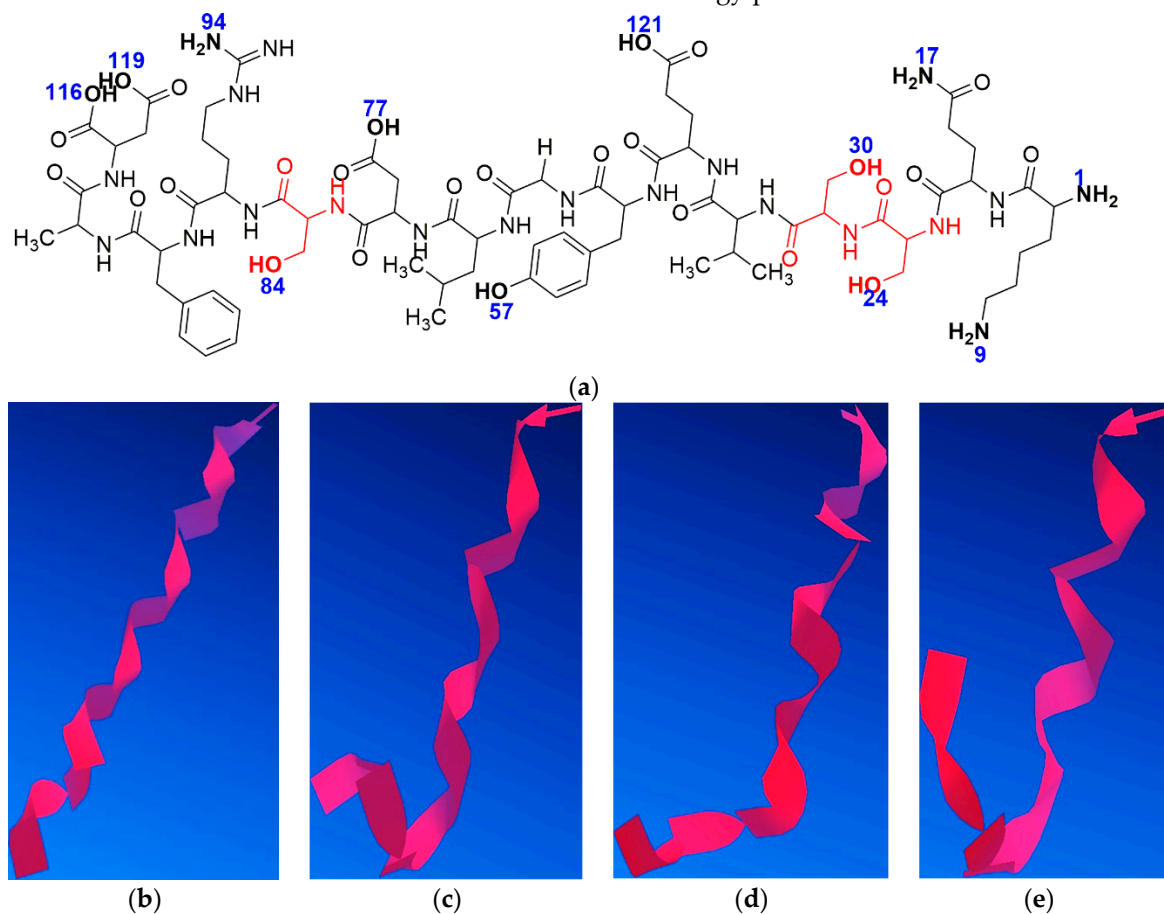
Coordination of Al ions to the N-terminus of $\text{A}\beta$ at the acidic residues Glu³, Asp⁷, and Glu¹¹ induces significant helical content, which means a major impact on the structure and dynamics of the peptide and reducing the impact of salt bridges, as well as the flexibility of binding residues and increasing that of terminal residues [23]. High helical content and disruption of salt bridges lead to a characteristic tertiary structure, as shown by heat maps of contact between residues, as well as representative clusters of trajectories [23]. The Al-induced flexibility allows for significant quantities of helical secondary structure to develop. Indeed, such metal ions affect residues 11–20 and 26–36 [23]. Salt bridges are strongly affected by the presence of the Al ion in the 11–16 region, as we demonstrated here. This, along with hydrogen bond patterns of serine-rich peptides that reflect the rather high helical content, lead to characteristic patterns in the tertiary structure in which stable contacts between salt-bridged pairs, as well as residues bound to Al ions, are apparent.

Therefore, FT-IR and CD are convenient methods to predict metal binding and conformational changes.

Although AD is not curable, some treatments are available to slow down the disease progression and reduce the cognitive impairment and behavioural problems, but do not stop the progression of neurodegeneration [38]. Our research may show new details about A β aggregation and fibrillation associated with AD and highlight the role of aluminium ions in creating a hydrophobic environment that increases the tendency of A β peptides to form plaques in AD brains.

The presented results are in good agreement with recent data demonstrating that the topology of A $\beta_{(1-16)}$ chelated with the Al³⁺ ion remains preserved, as compared to the free peptide [39], while another study performed with the A $\beta_{(1-28)}$ fragment revealed no measurable amounts of Al-peptide adducts upon peptide-metal mixing, regardless of experimental conditions [37]. We also considered that histidine residues are not involved in Al binding, but they may influence aluminium binding due to the rigidity of the peptide backbone.

The process of minimising peptide energy in silico was performed involving steric energy (Figure 15). For this study, the modified peptide A $\beta_{(1-16)}S_{3^6,13,14}$ was taken into consideration to understand the influence of the Al³⁺ ion on its secondary structure. Because serine residues introduced into the native A $\beta_{(1-16)}$ due to the hydroxyl group can form specific bonds with aluminium ions, we analysed the influence of these functional groups in complementarity with other amino and hydroxyl functions in the A $\beta_{(1-16)}$ secondary structure. We assumed that the two oxygen atoms of the hydroxyl groups of the two serine residues at positions 13 and 14 (atoms no. 24 and 30) bind to the Al³⁺ ion, while a third bond is formed between Al and the atom of oxygen or nitrogen from the amino and hydroxyl functional groups (numbered according to Figure 15a). Thus, we found 11 possible variants of such an interaction with Al. Each version was applied to the process of minimising energy in order to obtain the most stable conformation from the energy point of view.



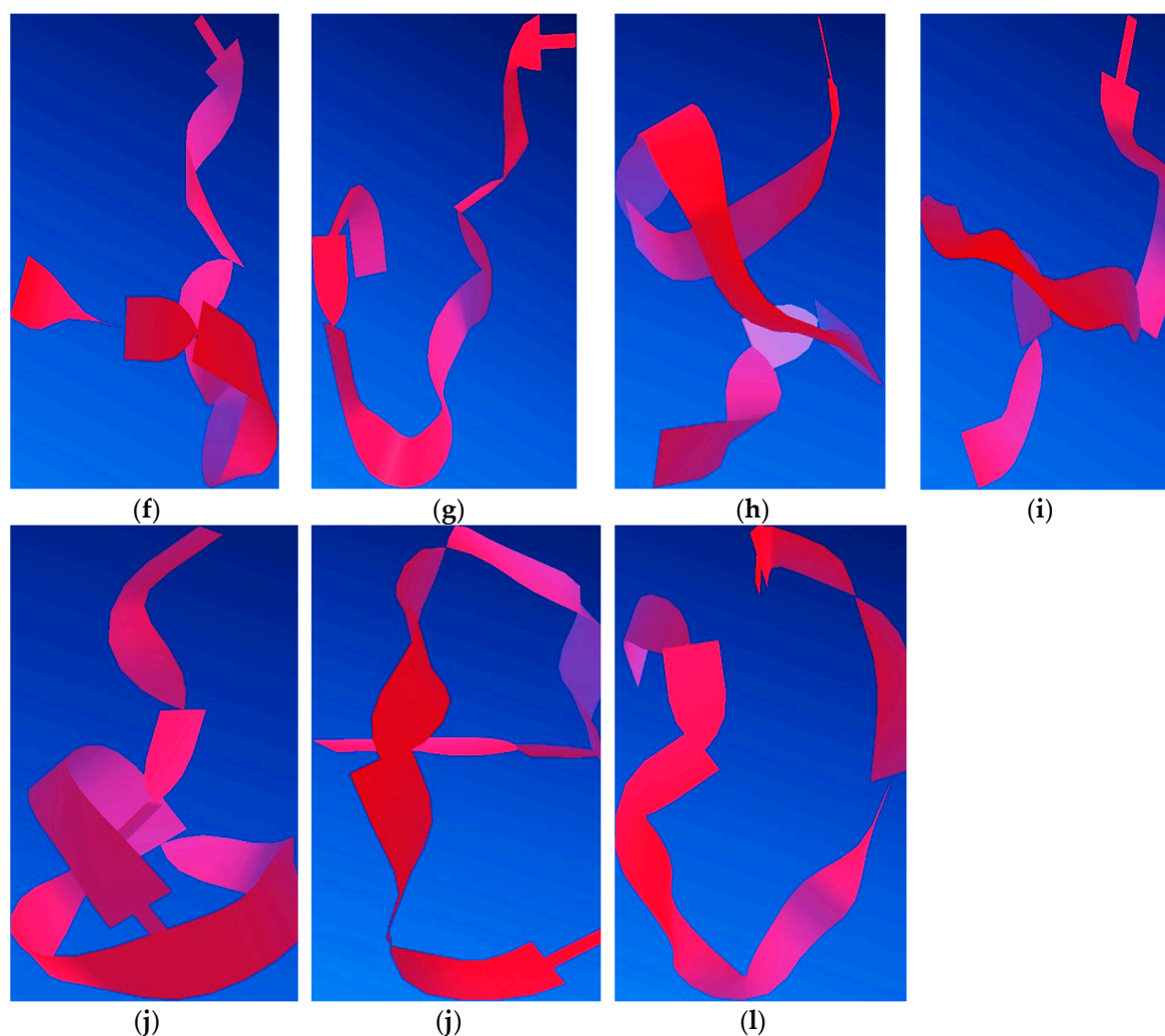


Figure 15. (a) $A\beta_{(1-16)}S_3^{6,13,14}$ sequence with the numbered atoms involved in the bonding process; (b) $A\beta_{(1-16)}S_3^{6,13,14}$; (c) $A\beta_{(1-16)}S_3^{6,13,14}(24.30)9$; (d) $A\beta_{(1-16)}S_3^{6,13,14}(24.30)1$; (e) $A\beta_{(1-16)}S_3^{6,13,14}(24.30)17$; (f) $A\beta_{(1-16)}S_3^{6,13,14}(24.30)121$; (g) $A\beta_{(1-16)}S_3^{6,13,14}(24.30)57$; (h) $A\beta_{(1-16)}S_3^{6,13,14}(24.30)77$; (i) $A\beta_{(1-16)}S_3^{6,13,14}(24.30)84$; (j) $A\beta_{(1-16)}S_3^{6,13,14}(24.30)116$; (k) $A\beta_{(1-16)}S_3^{6,13,14}(24.30)119$; (l) $A\beta_{(1-16)}S_3^{6,13,14}(24.30)94$.

Molecular modelling indicated that the site of aluminium binding migrates toward the C-terminus of the peptide, and the peptide backbone tends to adopt a rather β -sheet conformation, thus reducing the proportion of α -helix conformers that induced the specific elasticity of the peptide. Therefore, these findings suggest that with the interaction of aluminium ions with nitrogen and oxygen atoms, the rigidity of the structure increases, thus giving the peptide an attribute of inaccessibility to solvents, according to Figure 16. This may also suggest an increase in the hydrophobicity of the serine-rich peptide, which induces an increased tendency to aggregate. Nevertheless, we should keep in mind that a large proportion of $A\beta$ molecules are free and that a large amount of Al is unbound, acting in the form of inorganic compounds. These theoretical results confirm experimental CD, AFM, and FT-IR data.

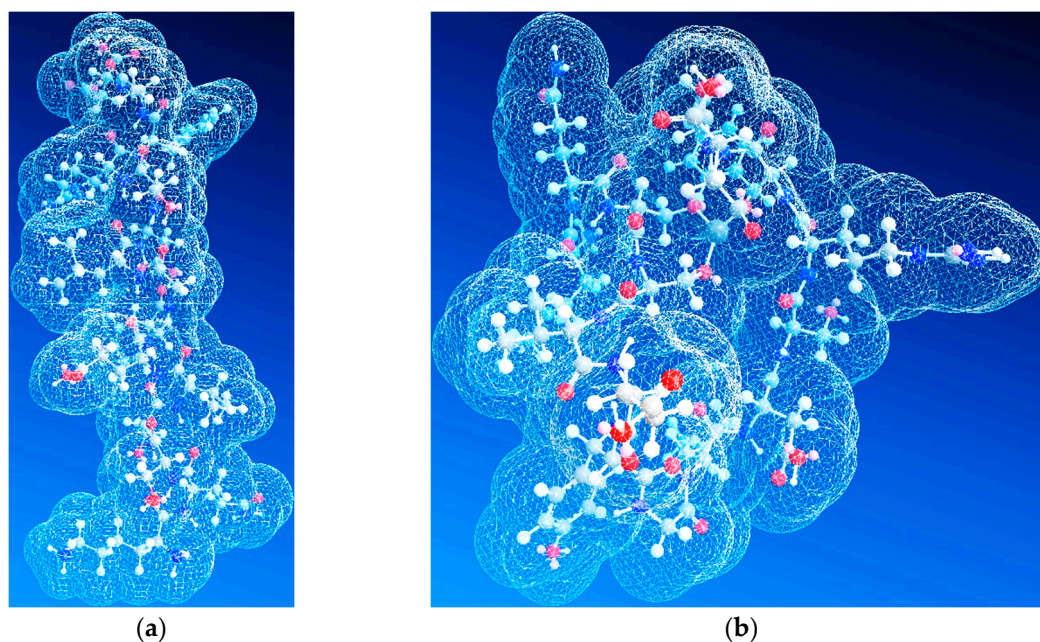


Figure 16. Accessibility of solvents to: (a) $A\beta_{(1-16)}S_3^{6,13,14}$; (b) $A\beta_{(1-16)}S_3^{6,13,14}(24.30)94 + Al^{3+}$.

4. Materials and Methods

All chemicals were of analytical or higher grade and purchased from well-recognised commercial sources. The solvents for peptide synthesis were commercial analytical grade and were redistilled before use. All solutions and buffers were prepared using MilliQ-grade water (18.2 M Ω -cm) from a Millipore water purification system (Milford, MA, USA). As solid support for the peptide synthesis, a Rink amide resin procured from Sigma-Aldrich Chemie GmbH was used (Taufkirchen, Germany). The following side chain-protected amino acids were used: Fmoc-Asp(OtBu)-OH, Fmoc-Ala-OH, Fmoc-Glu(OtBu)-OH, Fmoc-Phe-OH, Fmoc-Arg(Pbf)-OH, Fmoc-I-His(Trt)-OH, Fmoc-Ser(tBu)-OH, Fmoc-Gly-OH, Fmoc-I-Tyr(tBu)-OH, Fmoc-Val-OH, Fmoc-I-Gln(Trt)-OH, and Fmoc-Lys(Boc)-OH. Benzotriazol-1-yl-oxytripyrrolidino-phosphonium hexafluorophosphate (PyBOP) was used as an activator and purchased from Novabiochem (Darmstadt, Germany). Triisopropylsilan (TIS), dichloromethane (DCM), 4-methylmorpholine (NMM), piperidine, trifluoroacetic acid, and α -cyano-4-hydroxycinnamic acid (CHCA) were obtained from Sigma-Aldrich Ltd. (St. Louis, MO, USA). *N,N*-dimethylformamide (DMF) was purchased from Carl Roth (Karlsruhe, Germany), while ethanol and diethyl ether were achieved from Scharlab (Barcelona, Spain). Acetonitrile (ACN) was bought from Merck (Darmstadt, Germany). Deuterium oxide (D₂O) was supplied by Cambridge Isotope Laboratories, Inc. (Tewksbury, MA, USA), whereas aluminium sulphate and aluminium chloride were from Merck KGaA (Darmstadt, Germany). Piperidine (PYP) and bromophenol blue were obtained from Merck (Germany), while bradykinin, substance P, renin, adrenocorticotropin (ACTH), and oxidized insulin B-chain were from Sigma, city, Germany.

In addition to the peptides belonging to the $A\beta_{(1-16)}$ and $A\beta_{(9-16)}$ group, which were synthesised in our laboratory, other peptides and an amino acid were associated with the experiments of aluminium binding. The dipeptide glycyl-tyrosine (Gly-Tyr) was supplied by Fluka Chem. Co. (Steinheim, Germany) and chosen as a model for the $^9GY^{10}$ peptide fragment in the binding of aluminium ions. In addition, another dipeptide, seryl-glycine (Sigma), was used to study the behaviour of the system $^8SG^9$. Because the C-terminus of these two peptides is not amidated or protected, we also introduced in our experiments tyrosinamide (Tyr-NH₂) obtained from Sigma-Aldrich.

4.1. Synthesis of $A\beta$ Peptide Fragments

More detailed description of solid phase peptide synthesis was provided in our previous papers [30,32]. The sequence of $A\beta_{(1-16)}$ and those of the newly synthesised peptides were: $A\beta_{(1-16)}\text{:H-}^1\text{DAEFRHDSGYEVHHQK}^{16}\text{-NH}_2$, $A\beta_{(1-16)}A_{3^{6,13,14}}\text{:H-}^1\text{DAEFRADSGYEVAQAQK}^{16}\text{-NH}_2$, and $A\beta_{(1-16)}S_{3^{6,13,14}}\text{:H-}^1\text{DAEFRSDSGYEVSSQK}^{16}\text{-NH}_2$. The peptides were prepared by solid-phase peptide synthesis (SPPS) on a Fmoc Rink amide MBHA resin (MBHA, 4-methyl-benzohydroxymethyl-amine; 0.51 mmol g^{-1}) according to Fmoc/tBu chemistry, using an automated ResPepSL Peptide Synthesizer from Intavis (City, Germany). The synthesis protocol was as follows: (1) DMF washing, (2) Fmoc cleavage with 20% piperidine in DMF, (3) DMF washing, (4) coupling of Fmoc amino acid:PyBOP:NMM in DMF, and (5) DMF washing. Following the last amino acid loading to the chain, the Fmoc protecting group was removed and the peptide with a free amino terminal was washed with ethanol and DCM and subsequently subjected to lyophilisation until the next day. For the lyophilisation of peptides, a lyophiliser from Martin Christ Alpha 1-2 LDplus (Martin Christ, Osterode am Harz, Germany) was used. The peptides were cleaved from the resins at room temperature using a cleavage mixture consisting of 95% trifluoroacetic acid (TFA) as the cleavage agent, 2.5% triisopropylsilan, and 2.5% deionised water for 3 h. After cleavage, the peptides were precipitated with cold ($-20\text{ }^{\circ}\text{C}$) diethyl-ether overnight, then subjected to simple filtration. The solid material was dissolved in 5% aqueous solution of acetic acid prior to dry freezing.

The $A\beta_{(9-16)}$ peptide ($\text{H-}^9\text{GYEVHHQK}^{16}\text{-NH}_2$) and the modified peptides $A\beta_{(9-16)}G_1^{10}$ ($\text{H-}^9\text{GGEVHHQK}^{16}\text{-NH}_2$), $A\beta_{(9-16)}G_2^{13,14}$ ($\text{H-}^9\text{GYEVGGQK}^{16}\text{-NH}_2$), and $A\beta_{(9-16)}G_3^{10,13,14}$ ($\text{H-}^9\text{GGEVGGQK}^{16}\text{-NH}_2$) were manually synthesised by solid-phase peptide synthesis (SPPS) on a Fmoc Rink amide MBHA resin (0.48 mmol/g) according to Fmoc/tBu chemistry in a plastic syringe [40,41].

4.2. Reversed-Phase High-Performance Liquid Chromatography

$A\beta_{(1-16)}$ peptides were purified by an RP-HPLC SpectraSystem (Thermo Fisher Scientific, Dreieich, Germany) on a semi-preparative Vydac C8 column (250 mm \times 10 mm, 10 μm silica, and 300 \AA pore size) from Grace Columns. The mobile phase was a mixture of eluent A (0.1% TFA in water) and eluent B (0.1% TFA in acetonitrile–water (80:20, v/v)). A linear gradient elution was used for $A\beta$ separation (0 min 5% B; 5 min 5% B; 60 min 60% B; 65 min 100% B). A flow rate of 1.5 mL min^{-1} was used and the peptides were detected at 220 nm.

Analytical RP-HPLC was also performed on a SpectraSystem using an analytical Vydac C8 column (250 mm \times 4.6 mm) with 5 μm silica (300 \AA pore size) as a stationary phase (Grace Columns). The method was run at 1.0 mL min^{-1} using a mobile phase similar to the semi-preparative method.

Purification of $A\beta_{(9-16)}$ peptides was done by RP-HPLC on a UHPLC Dionex UltiMate 3000 instrument (Thermo Scientific, Bremen, Germany) on a Vydac C18 column (250 mm \times 4.6 mm), from Grace Columns, using two concentration gradients.

4.3. MALDI-ToF Mass Spectrometry

Matrix-assisted laser desorption/ionisation time-of-flight mass spectrometry (MALDI-ToF MS) analysis was carried out with a Bruker Ultraflex MALDI ToF/ToF mass spectrometer operated in positive reflectron mode and equipped with a pulsed nitrogen UV laser (Bruker Daltonics, Hamburg, Germany). For this analysis, the samples were co-crystallised with an excess of organic matrix capable of absorbing at 337 nm and volatilising under the action of laser radiation. As a matrix, a saturated solution of α -cyano-4-hydroxy-cinnamic acid (CHCA) dissolved in a solution containing 2:1 ACN:0.1% TFA in MilliQ was used for peptide mapping. Using the dried drop method, which implies adding first 1 μL of sample and over it 1 μL of freshly prepared matrix solution, the mixture was deposited on a conductive metallic plate called a target and allowed to dry. After co-crystallisation, the metal plate was introduced into the mass spectrometer and bombarded with short laser pulses. The desorbed and ionised molecules were accelerated by an electrostatic field and discharged through a high-fly metal flight tube. Depending on their mass, ionised molecules reached the detector at different times.

The spectra were recorded in positive reflectron mode using the following parameters: 20 kV acceleration voltage, 40% grid voltage, 140 ns delay, low-mass gate of 500 Da, and an acquisition mass

range of 600–3500 Da. The final mass spectrum represented an accumulation of 300 shots per acquisition. The obtained spectra were processed using Bruker's Flex Analysis 3.4 software.

4.4. ESI Type Mass Spectrometry

Electrospray ionisation ion trap mass spectra (ESI-MS) were recorded in positive mode by scanning from m/z 200 to m/z 2000 on an Esquire 3000+ ion trap mass spectrometer (Bruker Daltonik, Bremen, Germany). Each spectrum, corrected for the blank baseline, was the average of 15 scans. The ion source parameters were as follows: 19 psi nebulising gas (nitrogen), 9 L·min^{−1} of drying gas (nitrogen) at a dry temperature of 300 °C, capillary voltage 4000, skimmer −4V, and capillary exit 98.50 V. The flow rate of the sample was 600 µL h^{−1}. The collision-induced dissociation technique (CID) generated fragmentation of paternal ions. Collision-induced dissociation was done using argon as the target gas.

4.5. Peptide–Metal Complex Preparation

Al-Aβ_(9–16) peptide complex. A stock 384 µM solution of Aβ_(9–16) peptide and another one of 1.536 mM aluminium sulphate in ammonium acetate buffer (pH = 7.4) were prepared. To obtain 1:1 molar ratio solutions, 100 µL of 384 µM Aβ_(1–16) solution, 25 µL solution of 1.536 mM metal ions and 25 µL buffer solution were mixed in an Eppendorf vial. The peptide concentration in the final solution was 256 µM.

Al-Aβ_(1–16) peptide complexes. AFM and SEM studies were done using the native Aβ_(1–16) peptide and its variants with alanine and serine, Aβ_(1–16)A₃^{6,13,14}, and Aβ_(1–16)S₃^{6,13,14} at a concentration of 256 µM, treated with aluminium sulphate (1:1 and 1:2 molar ratios) for 24 h at 25 °C.

Al-Aβ_(9–16) peptide complexes. Separately, the newly synthesised, glycine-rich Aβ_(9–16) peptides were subjected to interaction with aluminium ions in aqueous AlCl₃ solutions in order to compare their affinity to Al with that of native Aβ_(9–16). Here, solutions of each Aβ_(9–16) peptide (8 mM) were mixed at pH 6.6 with aluminium chloride to obtain a peptide:metal ion molar ratio of 1:10. The resulting solutions were incubated (Thermomixer Compact Eppendorf AG 22331, City, Germany) for 20 h at 24 °C and 350 rpm. Finally, the samples were lyophilised and subjected to MS and FT-IR.

4.6. Circular Dichroism Spectroscopy (CD)

CD spectra were recorded on a Jasco J-720 spectropolarimeter (JASCO, Espoo, Finland) at room temperature in a 0.5 mm quartz cell under a constant stream of nitrogen (4 L/min). Buffer with ammonium acetate (15 mM) of pH 6.6 or pH 7.4 was used as the solvent. The Aβ_(1–16) peptide concentration was 256 µM. Spectra were the average of five scans between λ 180 and 260 nm. The results were expressed as molar ellipticity, after subtracting the buffer spectrum. A HANNA pH 211 microprocessor pH meter was used to measure the pH values.

4.7. Atomic Force Microscopy

In-phase and in-height AFM images were taken at room temperature (22 °C) on a SPM Solver PRO-M AFM (NT-MTD Co. Zelenograd, Moscow, Russia) using the tapping mode. All images were acquired using a high-resolution noncontact “Golden” silicon NSG10/Au/50 cantilever with Au conductive coating. The cantilever was 100 µm in length, 35 µm in width, 2 µm thick, and had a typical tip radius of 10 nm. A resonant frequency of 254 kHz and a force constant of 11.5 N m^{−1} were applied. All AFM images were obtained at a resolution of 256 × 256 pixels on a scale of 2 µm × 2 µm. We used AFM to characterise the film surface of native Aβ_(1–16) peptides in comparison with that of Aβ_(1–16)A₃^{6,13,14} and Aβ_(1–16)S₃^{6,13,14} upon incubation with aluminium at a concentration of 256 µM (1:1 and 1:2 molar ratios) for 24 h at 25 °C. To examine the topography of aggregates, two to three drops of each sample (approximately 50 µL of sample solution) were allowed to dry overnight on small glass slides in dust-free medium (covered with a Petri dish), at room temperature.

4.8. Scanning Electron Microscopy

A scanning electron microscope (SEM; Ultra plus Scanning Electron Microscope from Carl Zeiss NTS) (Manufacturer, City, State abbr. if USA, Country), operating at 4 kV with secondary electrons, in high-vacuum mode, was used to observe the morphological properties of the Al-peptide complexes. The SEM studies were performed on samples dried on small glass slides, fixed on copper supports using carbon tape, and covered with a thin layer of platinum to avoid electrostatic charging. We used SEM to characterise the fibril morphology of aggregates formed by $A\beta(1-16)A_3^{6,13,14}$ and $A\beta(1-16)S_3^{6,13,14}$ upon incubation with aluminium sulphate (peptide concentration 256 μ M; 1:1 molar ratio) for 24 h at 25 °C.

4.9. Fourier Transform Infrared Spectroscopy

The infrared spectra were measured using a Shimadzu 8400S FT-IR spectrophotometer (Shimadzu, Japan). The FT-IR spectra were recorded from 4000 to 400 cm^{-1} in spectroscopic-grade CsI with a detector at 2 cm^{-1} resolution and 20 scans per sample working in transmission mode. The collected FT-IR spectra were compared with the standard spectra of the functional groups.

4.10. NMR Spectroscopy

Proton NMR data were recorded by Dr. Catalina Ionica Ciobanu on a Bruker Avance III, 500 MHz frequency spectrometer, equipped with a 5 mm PABBO detection probe and operating at 500.19 MHz for ^1H nucleus. Chemical shifts are reported in δ units (ppm), relative to the solvent residual peak (D_2O , ^1H :4.79 ppm). Coupling constants are reported in Hertz (Hz). The number of scans for ^1H -NMR experiments was 256 and four scans for two-dimensional ^1H - ^1H NMR spectra. The peptide sample was prepared in D_2O as a solvent. The experiment was recorded without the introduction of a presaturation pulse for solvent signal suppression.

4.11. Data Analysis

The mass spectrometric data analyses were performed using the software Bruker Daltonics DataAnalysis 3.3. The molecular weight determination of peptides, as well as the prediction of the corresponding fragments in the MS/MS process of peptides and Al-fragment adducts, were conducted using GPMW 6.11 software (General Protein/Mass Analysis for Windows, Lighthouse Data, Odense M, Denmark) [42]. The monoisotopic peak list was compared against data calculated by GPMW. AFM image analysis was done with scanning probe microscopy software, WSxM 4.0 Develop 10.0 (NT-MTD Co. Zelenograd, Moscow, Russia). The obtained data following IR spectroscopy were processed using Origin software. Computer simulation was performed with the help of the Chem3D Ultra 10.0 program.

5. Conclusions

Our findings suggest that the N-terminal 1–16 sequence of $A\beta$ peptides has the is involved in aluminium ion binding associated with AD. The key observation in our study is that aluminium ions interact with the N-terminus $A\beta(1-16)$ sequence of amyloid- β peptides. In addition, the $A\beta(9-16)$ peptide fragment also interacts with Al, as the FT-IR experiments suggest. Consequently, several variants of $A\beta(1-16)$ and $A\beta(9-16)$ peptide fragments were synthesised and used to study their interaction with aluminium ions. These ions were suspected to induce the formation of $A\beta$ fibrils and aggregates. Through the formation of metal ion adducts during the MALDI-ToF MS measurements, we used MS/MS spectra to investigate aluminium binding to amyloid- β peptide fragments and analogues, and to identify the most probable binding sites. AFM images, as well as CD and FT-IR spectra, showed that the $A\beta(1-16)$ peptide conformation and fibrillation depend on the sequence of peptides and the presence of aluminium in solution. Free $A\beta(1-16)$ peptides, which are the hydrophilic N-terminus sequences of amyloid- β peptides, generated a smooth film surface because of their low tendency to aggregation. Instead, alanine-rich $A\beta(1-16)$ formed fibrils, most probably due to its hydrophobic characteristic, while serine-rich peptides had a pronounced tendency to fibrillation, probably due to the hydrogen bonding of serine residues. Aluminium ions induce peptide

aggregation and fibrillation, as demonstrated by AFM and SEM experiments. However, Al may have a higher affinity to amyloid peptides at a lower pH, and its binding could be pH dependent. Investigation of such short amyloid- β peptide fragments and analogues may provide clues for plaque formation under aggregation conditions and may facilitate the design of potential drugs for these targets. However, further research is needed to better understand the multiple interactions of aluminium ions with A β peptides for Alzheimer's disease.

Author Contributions: Conceptualisation, G.D.; methodology, G.D., C.S.M., and M.J.; software, C.S.M.; validation, G.D., C.S.M., and M.J.; formal analysis, G.D.; investigation, C.S.M. and M.J.; resources, G.D.; data curation, G.D.; writing—original draft preparation, G.D. M.J., and C.S.M.; writing—review and editing, G.D.; visualisation, G.D.; supervision, G.D.; project administration, G.D.; funding acquisition, G.D. and C.S.M. All authors have read and agreed to the published version of the manuscript.

Funding: This research received no external funding and the APC was funded by the Romanian Ministry of Research and Innovation, Program 1—Development of the national RD system, Subprogram 1.2—Institutional performance—RDI excellence funding projects, Grant no. 34PFE/19.10.2018.

Acknowledgments: We are grateful to the anonymous reviewers for insightful and constructive comments that greatly improved this manuscript. All authors appreciate the help by Catalina Ionica Ciobanu with NMR spectroscopy, Marcela Mihai with AFM and SEM images, and Laura Habasescu with A β _(1–16) peptide synthesis and characterisation. The authors are thankful for financial support from the Romanian Ministry of Research and Innovation, Program 1—Development of the national RD system, Subprogram 1.2—Institutional performance—RDI excellence funding projects, Grant no. 34PFE/19.10.2018.

Conflicts of Interest: The authors declare no conflict of interest. The funders had no role in the design of the study; in the collection, analyses, or interpretation of data; in the writing of the manuscript, or in the decision to publish the results.

Abbreviations

A β , amyloid- β peptide; AD, Alzheimer's disease; AFM, atomic force microscopy; Al, aluminium; CD, circular dichroism spectroscopy; FT-IR, Fourier transform infrared spectroscopy; SEM, scanning electron microscopy; SPPS, solid-phase peptide synthesis.

References

1. Fan, L.; Mao, C.; Xu, Y.; Shi, C.; Hu, X.; Zhang, S.; Dong, Y. New insights into the pathogenesis of Alzheimer's disease. *Front. Neurol.* **2019**, *10*, 1312, doi:10.3389/fneur.2019.01312.
2. Gao, J.; Wang, L.; Gao, C.; Arakawa, H.; Perry, G.; Wang, X. TDP-43 inhibitory peptide alleviates neurodegeneration and memory loss in an APP transgenic mouse model for Alzheimer's disease. *BBA-Mol. Basis Dis.* **2020**, *1866*, 165580, doi:10.1016/j.bbadis.2019.165580.
3. Peng, Y.; Gao, P.; Shi, L.; Chen, L.; Liu, J.; Long, J. Central and peripheral metabolic defects contribute to the pathogenesis of Alzheimer's disease. *Antioxid. Redox Sign.* **2020**, *32*, 1188–1236, doi:10.1089/ars.2019.7763.
4. Parodi-Rullán, R.; Sone, J.Y.; Fossati, S. Endothelial mitochondrial dysfunction in cerebral amyloid angiopathy and Alzheimer's disease. *J. Alzheimer's Dis.* **2019**, *72*, 1019–1039, doi:10.3233/JAD-190357.
5. Fontana, I.C.; Zimmer, A.R.; Rocha, A.S.; Gosmann, G. Souza DO, Lourenco MV, Zimmer ER. Amyloid- β oligomers in cellular models of Alzheimer's disease. *J. Neurochem.* **2020**, 1–22, doi:10.1111/jnc.15030.
6. van Dam, L.; Dansen, T.B. Cross-talk between redox signalling and protein aggregation. *Biochem. Soc. Trans.* **2020**, *48*, 379–397, doi:10.1042/BST20190054.
7. Yang, Z.; Song, Q.; Cao, Z.; Yu, G.; Liu, Z.; Tan, Z.; Deng, Y. Design, synthesis and evaluation of flurbiprofen-clioquinol hybrids as multitarget-directed ligands against Alzheimer's disease. *Bioorganic Med. Chem.* **2020**, *28*, 115374, doi:10.1016/j.bmc.2020.115374.
8. Scassellati, C.; Bonvicini, C.; Benussi, L.; Ghidoni, R.; Squitti, R. Neurodevelopmental disorders: Metallomics studies for the identification of potential biomarkers associated to diagnosis and treatment. *J. Trace Elem. Med. Biol.* **2020**, *60*, 126499, doi:10.1016/j.jtemb.2020.126499.
9. Bondy, S.C.; Campbell, A. Aluminium and neurodegenerative diseases. In *Advances in Neurotoxicology*; 1st ed.; Aschner, M., Costa, L.G., Eds.; Academic Press: Cambridge, MA, USA, 2017; Volume 3, pp. 131–156, doi:10.1016/bs.ant.2017.07.008.

10. Wallin, C.; Friedemann, M.; Sholts, S.B.; Noormägi, A.; Svantesson, T.; Jarvet, J.; Wärmländer, S.K. Mercury and Alzheimer's disease: Hg(II) ions display specific binding to the amyloid- β peptide and hinder its fibrillization. *Biomolecules* **2020**, *10*, 44, doi:10.3390/biom10010044.
11. Colautti, J.; Nagales, K. Tau and beta-amyloid in Alzheimer's disease: Theories, treatments strategies, and future directions. *Meducator* **2020**, *1*, 12–15, doi:10.35493/medu.37.12.
12. Moussa-Pacha, N.M.; Abidin, S.M.; Omar, H.A.; Alniss, H.; Al-Tel, T.H. BACE1 inhibitors: Current status and future directions in treating Alzheimer's disease. *Med. Res. Rev.* **2020**, *40*, 339–384, doi:10.1002/med.21622.
13. Bakulski, K.M.; Seo, Y.A.; Hickman, R.C.; Brandt, D.; Vadari, H.S.; Hu, H.; KyunPark, S. Heavy metals exposure and Alzheimer's disease and related dementias. *J. Alzheimer's Dis.* **2020**, *76*, 1215–1242, doi:10.3233/JAD-200282.
14. Kim, A.C.; Lim, S.; Kim, Y.K. Metal ion effects on A β and tau aggregation. *Int. J. Mol. Sci.* **2018**, *19*, 128, doi:10.3390/ijms19010128.
15. Gómez, M.; Esparza, J.L.; Cabré, M.; García, T.; Domingo, J.L. Aluminium exposure through the diet: Metal levels in A β PP transgenic mice, a model for Alzheimer's disease. *Toxicology* **2008**, *249*, 214–219, doi:10.1016/j.tox.2008.05.004.
16. Inan-Eroglu, E.; Ayaz, A. Is aluminium exposure a risk factor for neurological disorders? *J. Res. Med. Sci.* **2018**, *23*, 51, doi:10.4103/jrms.JRMS_921_17.
17. Lupaescu, A.V.; Humelnicu, I.; Petre, B.A.; Ciobanu, C.I.; Drochioiu, G. Direct evidence for binding of aluminium to NAP anti-amyloid peptide and its analogs. *Eur. J. Mass Spectrom.* **2020**, *26*, 106–116, doi:10.1177/1469066719877714.
18. Wang, Z.; Wei, X.; Yang, J.; Suo, J.; Chen, J.; Liu, X.; Zhao, X. Chronic exposure to aluminium and risk of Alzheimer's disease: A meta-analysis. *Neurosci. Lett.* **2016**, *610*, 200–206, doi:10.1016/j.neulet.2015.11.014.
19. Clauberg, M.; Joshi, J.G. Regulation of serine protease activity by aluminium: Implications for Alzheimer disease. *Proc. Natl. Acad. Sci. USA* **1993**, *90*, 1009–1012, doi:10.1073/pnas.90.3.1009.
20. Kandimalla, R.; Vallamkondu, J.; Corgiat, E.B.; Gill, K.D. Understanding aspects of aluminium exposure in Alzheimer's disease development. *Brain Pathol.* **2016**, *26*, 139–154, doi:10.1111/bpa.12333.
21. Mold, M.; Linhart, C.; Gómez-Ramírez, J.; Villegas-Lanau, A.; Exley, C. Aluminium and amyloid- β in familial Alzheimer's disease. *J. Alzheimer's Dis.* **2020**, *73*, 1627–1635, doi:10.3233/JAD-191140.
22. Pal, S.; Maity, S.; Sardar, S.; Parvej, H.; Das, N.; Chakraborty, J.; Halder, U.C. Curcumin inhibits the Al (iii) and Zn (ii) induced amyloid fibrillation of β -lactoglobulin in vitro. *RSC Adv.* **2016**, *6*, 111299–111307, doi:10.1039/C6RA24570F.
23. Turner, M.; Mutter, S.T.; Kennedy-Britten, O.D.; Platts, J.A. Molecular dynamics simulation of aluminium binding to amyloid- β and its effect on peptide structure. *PLoS ONE* **2019**, *14*, e0217992, doi:10.1371/journal.pone.0217992.
24. Ștefănescu, R.; Lupu, L.; Manea, M.; Iacob, R.E.; Przybylski, M. Molecular characterization of the β -amyloid(4–10) epitope of plaque specific A β antibodies by affinity-mass spectrometry using alanine site mutation. *J. Pept. Sci.* **2018**, *24*, e3047, doi:10.1002/psc.3047.
25. Ștefănescu, R.; Stanciu, G.D.; Luca, A.; Caba, I.C.; Tamba, B.I.; Mihai, C.T. Contributions of mass spectrometry to the identification of low molecular weight molecules able to reduce the toxicity of amyloid- β peptide to cell cultures and transgenic mouse models of Alzheimer's disease. *Molecules* **2019**, *24*, 1167, doi:10.3390/molecules24061167.
26. Mobed, A.; Hasanzadeh, M. The best alternative for conventional methods in detection of Alzheimer's disease biomarkers. *Int. J. Biol. Macromol.* **2020**, *161*, 59–71, doi:10.1016/j.ijbiomac.2020.05.257.
27. Ji, W.; Yuan, C.; Chakraborty, P.; Makam, P.; Bera, S.; Rencus-Lazar, S.; Li, J.; Yan, X.; Gazit, E. Co-assembly induced transformation of dipeptide amyloid-like structures into stimuli-responsive supramolecular materials. *ACS Nano* **2020**, *14*, 7181–7190, doi:10.1021/acsnano.0c02138.
28. Prado-Audelo, D.; María, L.; Caballero-Florán, I.H.; Meza-Toledo, J.A.; Mendoza-Muñoz, N.; González-Torres, M.; Leyva-Gómez, G. Formulations of curcumin nanoparticles for brain diseases. *Biomolecules* **2019**, *9*, 56, doi:10.3390/biom9020056.
29. Lermyte, F.; Everett, J.; Lam, Y.P.; Wootton, C.A.; Brooks, J.; Barrow, M.P.; Collingwood, J.F. Metal ion binding to the amyloid β monomer studied by native top-down FTICR mass spectrometry. *J. Am. Soc. Mass Spectrom.* **2019**, *30*, 2123–2134, doi:10.1021/jasms.8b06229.

30. Murariu, M.; Habasescu, L.; Ciobanu, C.I.; Gradinaru, R.V.; Pui, A.; Drochioiu, G.; Mangalagiu, I. Interaction of amyloid A β (9–16) peptide fragment with metal ions: CD, FT-IR, and fluorescence spectroscopic studies. *Int. J. Pept. Res. Ther.* **2019**, *25*, 897–909, doi:10.1007/s10989-018-9738-1.
31. Jureschi, M.; Lupaescu, A.V.; Ion, L.; Petre, B.A.; Drochioiu, G. Stoichiometry of heavy metal binding to peptides involved in Alzheimer's disease: Mass spectrometric evidence. *Adv. Exp. Med. Biol.* **2019**, *1140*, 401–415, doi:10.1007/978-3-030-15950-4_23.
32. Habasescu, L.; Jureschi, M.; Petre, B.A.; Mihai, M.; Gradinaru, R.V.; Murariu, M.; Drochioiu, G. Histidine-lacked A β (1–16) peptides: pH-dependent conformational changes in metal ion binding. *Int. J. Pept. Res. Ther.* **2020**, 1–18, doi:10.1007/s10989-020-10048-0.
33. Stroo, E.; Koopman, M.; Nollen, E.A.; Mata-Cabana, A. Cellular regulation of amyloid formation in aging and disease. *Front. Neurosci.* **2017**, *11*, 64, doi:10.3389/fnins.2017.00064.
34. Kepp, K.P. Alzheimer's disease: How metal ions define β -amyloid function. *Coord. Chem. Rev.* **2017**, *351*, 127–159, doi:10.1016/j.ccr.2017.05.007.
35. Nayak, P. Aluminium: Impacts and disease. *Environ. Res.* **2002**, *89*, 101–115, doi:10.1006/enrs.2002.4352.
36. Istrate, A.N.; Tsvetkov, P.O.; Mantsyzov, A.B.; Kulikova, A.A.; Kozin, S.A.; Makarov, A.A.; Polshakov, V.I. NMR solution structure of rat A β (1–16): Toward understanding the mechanism of rats' resistance to Alzheimer's disease. *Biophys. J.* **2012**, *102*, 136–143, doi:10.1016/j.bpj.2011.11.4006.
37. Valensin, D.; Migliorini, C.; Valensin, G.; Gaggelli, E.; La Penna, G.; Kozlowski, H.; Gabbiani, C.; Messori, L. Exploring the reactions of β -amyloid (A β) peptide 1–28 with Al^{III} and Fe^{III} ions. *Inorg. Chem.* **2011**, *50*, 6865–6867, doi:10.1021/ic201069v.
38. Agnihotri, A.; Aruoma, O.I. Alzheimer's disease and Parkinson's disease: a nutritional toxicology perspective of the impact of oxidative stress, mitochondrial dysfunction, nutrigenomics and environmental chemicals. *J. Am. College Nutr.* **2020**, *39*, 16–27, doi:10.1080/07315724.2019.1683379.
39. Narayan, P.; Krishnarajuna, B.; Vishwanathan, V.; Jagadeesh Kumar, D.; Babu, S.; Ramanathan, K.V.; Raghothama, S. Does aluminium bind to histidine? An NMR investigation of amyloid β 12 and amyloid β 16 fragments. *Chem. Biol. Drug Des.* **2013**, *82*, 48–59, doi:10.1111/cbdd.12129.
40. Coin, I.; Beyermann, M.; Bienert, M. Solid-phase peptide synthesis: From standard procedures to the synthesis of difficult sequences. *Nat. Protoc.* **2007**, *2*, 3247–3256, doi:10.1038/nprot.2007.454.
41. Amblard, M.; Fehrentz, J.A.; Martinez, J.; Subra, G.; Methods and protocols of modern solid phase peptide synthesis. *Mol. Biotechnol.* **2006**, *33*, 239–254, doi:10.1385/MB:33:3:239.
42. Peri, S.; Steen, H.; Pandey, A. GPMAW—a software tool for analyzing proteins and peptides. *Trends Biochem. Sci.* **2001**, *26*, 687–689, doi:10.1016/S0968-000401954-5.

Sample Availability: Samples of the compounds are not available from the authors.



© 2020 by the authors. Licensee MDPI, Basel, Switzerland. This article is an open access article distributed under the terms and conditions of the Creative Commons Attribution (CC BY) license (<http://creativecommons.org/licenses/by/4.0/>).